Inorganic Chemistry

pubs.acs.org/IC Article

Siamese-Twin Porphyrin Goes Platinum: Group 10 Monometallic, Homobimetallic, and Heterobimetallic Complexes

Sarina J. Dorazio, Anastasia Vogel, Sebastian Dechert, Dustin E. Nevonen, Victor N. Nemykin,* Christian Brückner,* and Franc Meyer*

Cite This: https://dx.doi.org/10.1021/acs.inorgchem.0c00714 Read Online

ACCESS | Metrics & More | Article Recommendations | Supporting Information

ABSTRACT: A series of Pt^{II}-based monometallic (**H_2PtL**), homobimetallic (**Pt_2L**), and heterobimetallic (**NiPtL** and **PdPtL**) group 10 complexes of the previously established expanded twin porphyrin (**H_4L**) were prepared. Structural characterization of the bimetallic Pt^{II} series (**Pt_2L**, **NiPtL**, and **PdPtL**) revealed their similar general structures, with slight differences correlated to the ion size. An improvement of the metal-ion insertion process also allowed efficient preparation of the known **Pd_2L** complex, and the novel heterobimetallic **NiPdL** complex was also structurally characterized. UV−vis spectroscopy, NMR spectroscopy, magnetic circular dichroism (MCD), and (spectro)electrochemistry were used to characterize the complexes; the electronic properties followed largely established lines for metal complexes of the twin porphyrin, except that the Pt^{II}-based systems exhibited more complex UV−vis spectral signatures. MCD spectra accompanied by density functional theory (DFT)/time-dependent DFT computations rationalize the origins of the optical features of the twin porphyrin due to the presence of nonplanar, nonaromatic macrocyclic π systems that are more localized on half of the molecule and significant pyrazole(π) → pyrrole(π^*) intramolecular charge-transfer character. This study adds to our fundamental understanding of the formation, structure, and electronic structure of bimetallic complexes of this class of expanded metalloporphyrins containing nonpyrrolic moieties.

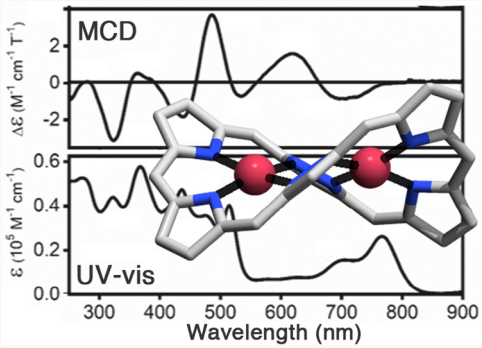

■ INTRODUCTION

Expanded porphyrins are porphyrin-inspired oligopyrrolic macrocycles of at least 17 internal ring atoms.[1−6] Such an expansion may introduce, inter alia, conformational flexibility into the macrocycle, enlarge its metal binding cavity, or increase the number of donor atoms for the complexation of one or more metal ions. Most expanded porphyrins rely on increasing the number of pyrrolic building blocks linked either directly via α−α linkages or through one C atom, such as the classic sapphyrin,[7,8] hexaphyrin **$H_2$1**,[9−13] octaphyrin **$H_4$2**,[14−16] or even larger architectures (Figure 1).[5,6] Nonpyrrolic heterocycles (e.g., thiophene, furan, pyridine, or pyrazole)[8,17−23] or conjugated spacers such as phenylene[24] or ferrocene[25] may be incorporated into the macrocycle, illustrating the broad diversity of molecules classified as expanded porphyrins.

An abundance of main-group, d-block, and f-block metal ions coordinate to expanded porphyrins,[26,27] mirroring the versatility of porphyrinic ligands while providing further insight into aromaticity, morphology, and electronic communication.[5,28−31] Changes in the macrocycle topology upon metal-ion complexation are reflected in the frequently much altered electronic properties of the macrocycle, as measured by UV−vis and NMR spectroscopy or electrochemistry.[5,28−31]

We previously introduced Siamese-twin porphyrin **H_4L** as a nonaromatic, nonplanar expanded porphyrin incorporating two pyrazole moieties that bridge two porphyrin-like N_4 binding pockets[19,32] that are suitable for the coordination of one or two metal ions.[19,32−34] The periphery of **H_4L** is decorated with phenyl and ethyl groups, enforcing a helimeric twist that is rigidified and modulated upon metal-ion complexation. The structure of **H_4L** is reminiscent of hexaphyrin **$H_2$1** due to the arrangement of six heterocycles with aryl groups at each meso position[12,35,36] but more closely resembles octaphyrin **$H_4$2**[1] in its mode of all-nitrogen coordination to metal ions (**$M_2$2** and **M_2L**).[37−39] Metalation of both octaphyrin **2** and twin porphyrin **H_4L** is facilitated by the steric constraints imposed by the peripheral substituents that force all coordinating N atoms toward the center of the cavity.[19,32]

Variation of the *meso*-aryl groups in twin porphyrin **H_4L** only negligibly altered the optical absorbance and redox

Received: March 9, 2020

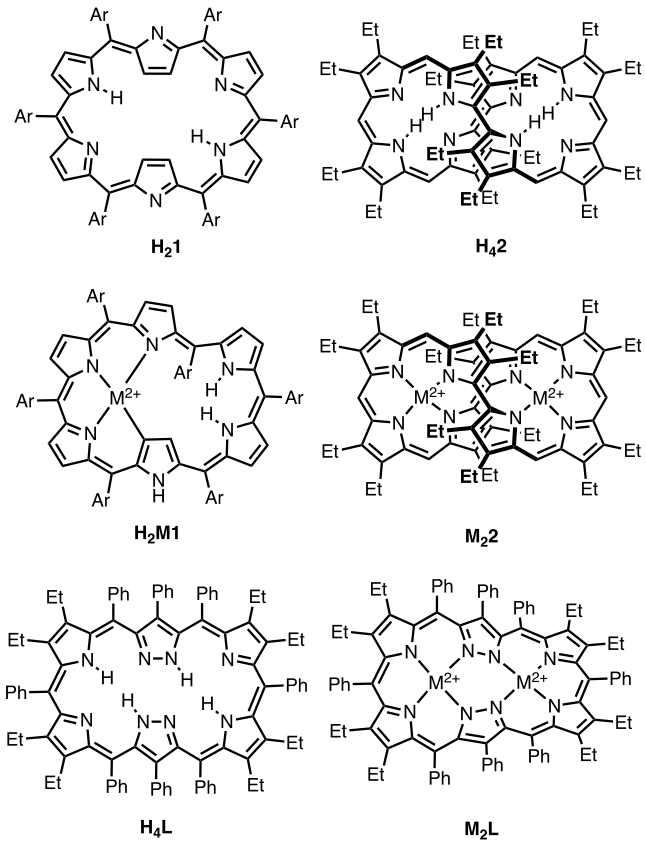

Figure 1. Representative expanded porphyrins and their metal complexes: a hexaphyrin **$H_2$1** and its metal complexes **H_2M1**, an octaphyrin **$H_4$2** and its metal complexes **$M_2$2**, and the Siamese-twin porphyrin **H_4L** and its metal complexes **M_2L**.

properties, reflecting the orthogonality of the aryl π system and the macrocycle mean plane.[33] Efforts to oxidize the macrocycle to achieve a fully aromatic system resulted instead in fused and folded "origami" structures.[40] The use of different metal ions produced more spectral and electrochemical changes than aryl substitution,[33,41,42] leading to studies of monometallic and bimetallic complexes of twin porphyrin **H_4L** (i.e., **H_2NiL**, **H_2PdL**, **Ni_2L**, **Cu_2L**, and **NiCuL** complexes),[19,32−34,41,42] establishing the twin porphyrin macrocycle as a noninnocent ligand capable of undergoing ligand-centered oxidations.[41,42] The remarkable stability of monometallic **H_2PdL** toward oxidation and reduction allowed for electrochemical, spectroelectrochemical, and electron paramagnetic resonance (EPR) studies of the oxidized/reduced species as well as investigations into its acid−base properties, providing further insight into the conjugated, yet electronically distinct, halves of the macrocycle.[34]

Platinum(II) and palladium(II) porphyrinoids have found utility as optical oxygen sensors related to technical and biological applications,[43−48] as photosensitizers for isomerization processes[49] and photodynamic therapy,[50,51] as photocatalysts for CH activation,[52] and as luminophores with high quantum yield [sometimes also emitting in the near-IR (NIR)].[53−55] In this contribution, we expand the investigation of the twin porphyrin metal complexes to Pt^{II}-based monometallic and bimetallic complexes of the group 10 metals (**H_2PtL**, **Pt_2L**, **NiPtL**, and **PdPtL**), as well as the new heterobimetallic complex **NiPdL**. Thus, in combination with the **H_2NiL**,[42] **H_2PdL**,[34] **Ni_2L**,[42] and **Pd_2L**[34] complexes prepared previously, the entire series of monometallic and bimetallic complexes of the group 10 metals with all possible combinations of Ni^{II}, Pd^{II}, and Pt^{II} are now available to further probe structure−function relationships of the twin porphyrins, particularly their optical and redox properties as a function of the chelated metal ions. The diamagnetic nature of the square-planar geometry of these low-spin d^8 metal ions allows their solution-state structures to be probed using NMR spectroscopy. The series of complexes prepared also proved suitable for magnetic circular dichroism (MCD) spectral analysis combined with time-dependent density functional theory (TDDFT) computations to illuminate in greater detail the origins of their optical spectra.

RESULTS AND DISCUSSION

Synthesis of the Complexes. The twin porphyrin ligand **H_4L**, synthesized according to established routes,[19,32,40] was mono- and bis-metalated with M = Ni^{II}/Pd^{II} using their acetate salts (Scheme 1). Use of the higher-boiling solvent 1,2-dichloroethane ($C_2H_4Cl_2$-1,2) proved advantageous and allowed us to readily prepare the known complexes **Ni_2L**[42] and **Pd_2L**[34] more rapidly or in better yields (for experimental details, see the Experimental Section and Supporting Information). This solvent also allowed us to introduce Pt^{II} into the macrocycle to prepare the novel monometallic species **H_2PtL** and its corresponding homobimetallic analogue **Pt_2L** using PtI_2/NaOAc. Complexation of Pt^{II} was noticeably slower (8 h) than that of Ni^{II} (2 h)[42] and Pd^{II} (1 h).[34] A combination of metal salt solubility and intrinsic kinetic factors of the metal ions rationalize these differences.

The progress of metal ion insertion was monitored with thin-layer chromatography (TLC), which indicated that the monometallic species formed before the bimetallic species, as expected. To promote monometalation, the known complexes **H_2NiL** and **H_2PdL** were prepared at ambient temperature, while the preparation of **H_2PtL** required reflux conditions. The latter reaction was carefully monitored with TLC to minimize the formation of **Pt_2L**. After isolation of the platinum complexes **H_2PtL** and **Pt_2L** in good yields using silica gel chromatography, analytical and spectroscopic data confirmed their expected compositions and connectivities (for details, see the Experimental Section and Supporting Information).

The novel heterobimetallic species **NiPtL**, **NiPdL**, and **PdPtL** were prepared from the isolated monometallic species (Scheme 1), whereby two alternative routes are available: insertion of the heavier metal preceding that of the lighter metal, or vice versa. In general, we find that insertion of the heavier, kinetically more inert metal species, followed by the lighter metal species, is more advantageous in terms of yields and reaction times than the alternate route. This likely reflects that insertion of the first metal rigidifies the macrocycle, thereby restricting insertion of a second metal ion, which is less deleterious when the second metal ion for insertion is more labile. Use of $C_2H_4Cl_2$-1,2 alone or $C_2H_4Cl_2$-1,2 with either ethanol (EtOH) or acetonitrile (MeCN) further facilitated insertion by providing good solubility of the twin porphyrin and metal salts while also allowing reflux at higher temperature than either dichloromethane (CH_2Cl_2) or chloroform ($CHCl_3$) with methanol (MeOH). The heterobimetallic complexes formed could be isolated with silica gel chromatography in good yields and showed all of the expected analytical and spectroscopic properties (for details, see the Experimental Section and Supporting Information).

https://dx.doi.org/10.1021/acs.inorgchem.0c00714
Inorg. Chem. XXXX, XXX, XXX−XXX

Scheme 1. Synthetic Routes to the Group 10 Twin Porphyrin Complexes[a]

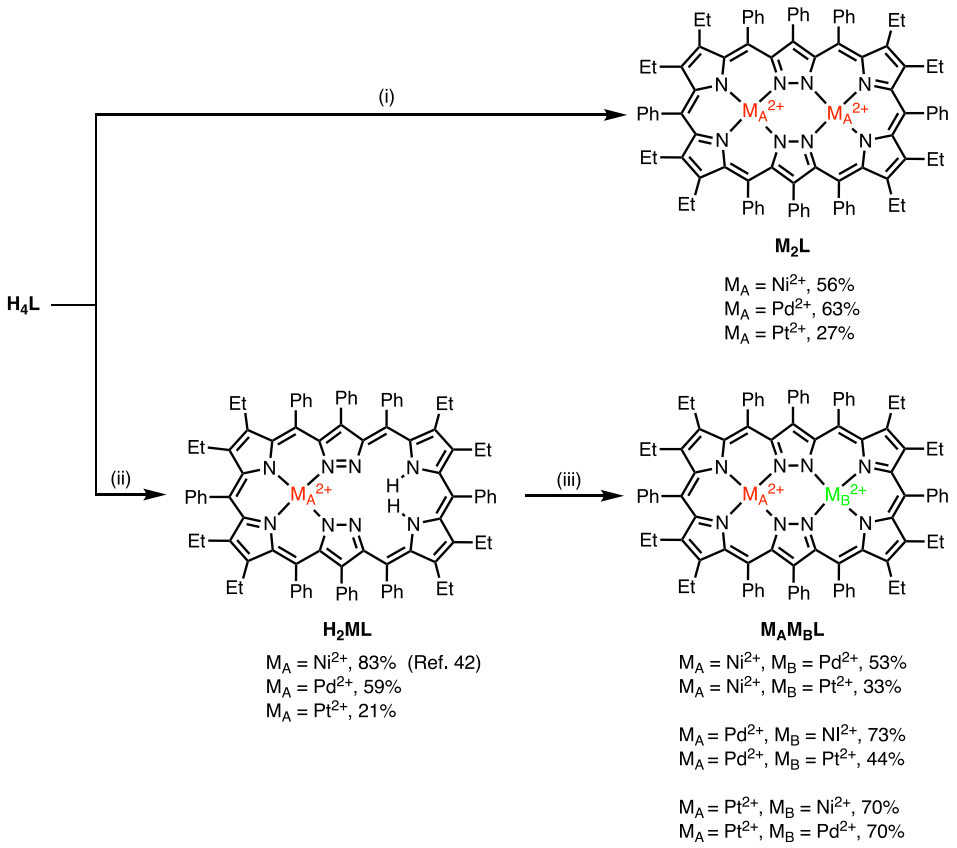

[a](i) **Ni_2L**: $Ni(OAc)_2$, $C_2H_4Cl_2$-1,2/EtOH, Δ, 2 h. **Pd_2L**: $Pd(OAc)_2$, $C_2H_4Cl_2$-1,2, Δ, 1 h. **Pt_2L**: PtI_2/NaOAc, $C_2H_4Cl_2$-1,2/MeCN, Δ, 8 h. (ii) **H_2NiL**: $Ni(OAc)_2$, CH_2Cl_2/MeOH, rt, 15 min; **H_2PdL**: $Pd(OAc)_2$, CH_2Cl_2, rt, 5 h; **H_2PtL**: PtI_2/NaOAc, $C_2H_4Cl_2$-1,2/MeCN, Δ, 4 h. (iii) **NiPdL**: H_2NiL, $Pd(OAc)_2$, $C_2H_4Cl_2$-1,2, Δ, 1 h or H_2PdL, $Ni(OAc)_2$, $C_2H_4Cl_2$-1,2/EtOH, Δ, 10 min; **NiPtL**: H_2NiL, PtI_2/NaOAc, $C_2H_4Cl_2$-1,2/MeCN, Δ, 21 h or H_2PtL, $Ni(OAc)_2$, $C_2H_4Cl_2$-1,2/EtOH, Δ, 10 min. **PdPtL**: H_2PdL, PtI_2/NaOAc, $C_2H_4Cl_2$-1,2/MeCN, Δ, 6 h or H_2PtL, $Pd(OAc)_2$, $C_2H_4Cl_2$-1,2, Δ, 10 min.

Solid-State Conformations. All compounds for which solid-state structures could be determined (**NiPdL**, **NiPtL**, **PdPtL**, and **Pt_2L**) show the characteristic twisted conformation intrinsic to the free base **H_4L** (in its diprotonated form),[40] as well as all other protonated or metalated twin porphyrin species structurally characterized to date (Figure 2A).[19,32,34,41] All compounds are essentially isostructural (Figure 2B). The small differences in their conformations largely reflect the size of the square-planar-coordinated d^8 ions [Ni^{II} (0.63 Å) < Pt^{II} (0.74 Å) < Pd^{II} (0.78 Å)].[56] Thus, the average M−N bond lengths for the homobimetallic complexes are shortest for Ni^{II} (Ni−N_{avg} 1.91 Å), longer for Pt^{II} (Pt−N_{avg} 2.01 Å), and longest for Pd^{II} (Pd−N_{avg} 2.03 Å) (Table 1). The nearly ideal square-planar geometry can be quantified using the structural index parameter τ_4 (where a value of 0 represents perfect square plane and a value of 1 a tetrahedral coordination sphere);[57] τ_4 values for the homobimetallic complexes **Ni_2L**,[42] **Pt_2L**, and **Pd_2L** are 0.19 for Ni^{II}, 0.17 for Pt^{II}, and 0.13 for Pd^{II}, respectively, with Pd^{II} possessing a coordination sphere that is least distorted from square planar. In regular porphyrins, Ni^{II} often leads to ruffled macrocycle conformations that reduce the Ni−N bond lengths to better accommodate the small metal ion (with Ni−N distances typically ∼1.93 Å),[58−60] while not substantially distorting the {N_4} coordination sphere. Adjustment of the degree of the twist modality inherent to the twin porphyrin framework allows for a slight shortening of the Ni−N bond lengths (or, more generally, a narrowing of the N−N distance between opposite N-donor pairs) but at the expense of the degree of deviation from a perfectly square-planar coordination sphere. The slightly more twisted conformation of the nickel complex **Ni_2L** compared to that of the two heavier homobimetallic congeners **Pd_2L** and **Pt_2L** (as well as quite similar heterobimetallic **PdPtL**) is also expressed in the metric parameters that define the macrocycle helimeric twist,[32] i.e., the torsion angles along the long axis (τ_{long}, between 93 and 106°) and along the short pyrazole axis (τ_{short}, between 70 and 76°).

An exact metric analysis of the heterobimetallic complexes is hampered by disorder of both metals over both positions, resulting in only average bond lengths for the crystallographically determined structures in the solid state. Furthermore, depending on the mode of preparation, we also observed noninteger occupancy of the metal ion positions that deviated from the expected 1:1 metal ion distribution, based on mass spectrometry analyses (estimated **$Ni_{1.22}Pd_{0.78}L$**, **$Ni_{1.15}Pt_{0.85}L$**, and **$Pd_{1.17}Pt_{0.83}L$**). Nonetheless, the alternating C−C bond lengths indicative of the nonaromatic π-system inherent to the twin porphyrin macrocycle can be distinguished (Figure 2C).

NMR Spectroscopic Characterization. The low-spin, square-planar d^8 metal ions Ni^{II}, Pd^{II}, and Pt^{II} are all diamagnetic, making the series of complexes prepared ideal for study by ^1H, ^{13}C, and ^{195}Pt NMR spectroscopy. Unlike the

https://dx.doi.org/10.1021/acs.inorgchem.0c00714
Inorg. Chem. XXXX, XXX, XXX−XXX

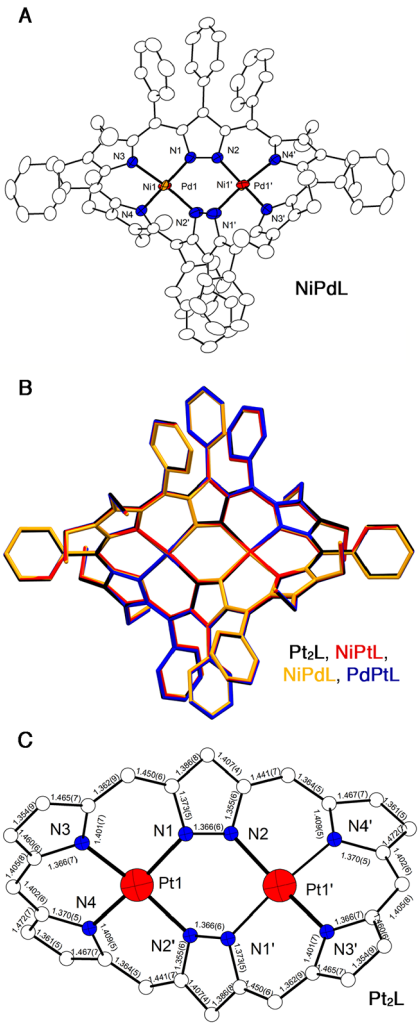

Figure 2. (A) Plot of the molecular structure of **NiPdL**. (B) Overlay of the molecular structures of **Pt_2L** (black), **NiPtL** (red), **NiPdL** (orange), and **PdPtL** (blue). H atoms are omitted. (C) Macrocycle framework bond lengths (Å) observed for **Pt_2L**. For details on the X-ray diffraction studies and bond-length analyses of **NiPtL**, **NiPdL**, and **PdPtL**, see the Supporting Information.

conformationally flexible and dynamic (on the NMR time scale at ambient temperature) free-base ligand **H_4L**,[32] well-resolved NMR spectra of the bimetallic complexes **Pd_2L**, **Pt_2L**, **NiPtL**, **PdPtL**, and **NiPdL** (and diprotonated **H_4PtL^{2+}**) could be obtained at 298 K, indicative of significant rigidification upon metal complexation (and protonation; Figure 3). The limited solubility of **Pt_2L** complicated the collection of ^{13}C NMR spectra for this species (for details, see the Supporting Information).

The helimerically twisted homobimetallic species (**Ni_2L**, **Pd_2L**, and **Pt_2L**) are D_2-symmetric, with C_2-symmetric rotation through both the long axis (i.e., viewed down the mes positions of the dipyrromethene locations of the molecule) as well as a second C_2-symmetric rotation through the shorter pyrazole axis (noncrystallographic symmetries). Interpretation of the NMR data of the metal complexes indicates that the helimeric twist observed in the solid state is also preserved in solution; this results in the manifestation of NMR signals from only one-quarter of the molecule with clearly distinct nonequivalent phenyl and ethyl groups. The monometallic species **H_2PtL** and the heterobimetallic species **NiPtL** and **PdPtL** (and **NiPdL**; see the Supporting Information) lost their symmetry along the short axis, with a corresponding doubling of the NMR signals. Protonation of **H_2PtL** with trifluoroacetic acid (TFA; at 268 K) resolves the very broad NH signal of the neutral species, but its ^{13}C, 2D, and ^{195}Pt NMR spectra suggest the presence of protonated species, likely a mixture of the mono- and diprotonated species (**H_3PtL^+** and **H_4PtL^{2+}**), as was also observed for **H_2NiL**.[34,42]

The Pt^{II}-containing complexes do not exhibit any hyperfine $^{195}Pt-^{1}H$ or $^{195}Pt-^{13}C$ couplings, likely due to the Pt^{II} coordination sphere comprised solely of four quadrupolar (^{14}N) N atoms that contribute to the expression of relatively broad signals (see the Supporting Information) because the ^{195}Pt nucleus is very sensitive to changes in its coordination environment. The typical range of chemical shifts for Pt^{II} coordinated to four N-donor ligands is between −2795 and −2145 ppm,[61] whereas the range of some aromatic Pt^{II} metalloporphyrins was shown to lie between +1235 and +1315 ppm;[62] the large diatropic ring current induced by the aromatic π system of porphyrins causes this large shift of the signal. Chemical shifts of the bimetallic Pt^{II}-containing twin porphyrin complexes **NiPtL**, **PdPtL**, and **Pt_2L** fall within the range of typical N_4 donors (−2519 to −2372 ppm), highlighting the lack of a macrocyclic ring current. Variation of the observed ^{195}Pt NMR signals is a result of nuanced distortions of the Pt^{II} coordination sphere and the non-equivalent electronic environments (varying distances of M−Pt separation and different M atoms in the **NiPtL**, **PdPtL**, and **Pt_2L** complexes; cf. Table 1).

UV−Vis Spectra. As is characteristic for the nonaromatic macrocyclic twin porphyrins and their metal complexes,[19,32−34,40−42] the UV−vis spectra of the group 10 twin porphyrin complexes more closely resemble those of linear

Table 1. Selected Bond Lengths and Angles of Bimetallic Group 10 Complexes and Structural Index Parameters for the Metal Ions

	M−N_{avg} (Å)	τ_4 [a]	d_{long} (Å)	τ_{tong} [b] (deg)	d_{short} (Å)	τ_{short} [c] (deg)	M−M (Å)	ref
Ni_2L	1.91	0.19	10.48	106	6.92	76	3.81	42
Pd_2L	2.03	0.13	10.68	93	7.09	71	3.93	34
Pt_2L	2.01	0.17	10.67	95	7.09	70	3.92	this work
NiPdL	1.95	0.16	10.64	99	6.94	74	3.85	this work
NiPtL	1.95	0.17	10.57	99	6.97	73	3.88	this work
PdPtL	2.01	0.15	10.68	94	7.09	70	3.92	this work

[a]The heterobimetallic τ_4 values are an average for both metal ions. [b]Torsion angle measured from the dipyrromethene α-pyrrole/α-pyrrole to opposite the dipyrromethene α-pyrrole/α-pyrrole. [c]Torsion angle measured from the pyrazole 3 and 5 positions to the opposite pyrazole 3 and 5 positions.

https://dx.doi.org/10.1021/acs.inorgchem.0c00714
Inorg. Chem. XXXX, XXX, XXX−XXX

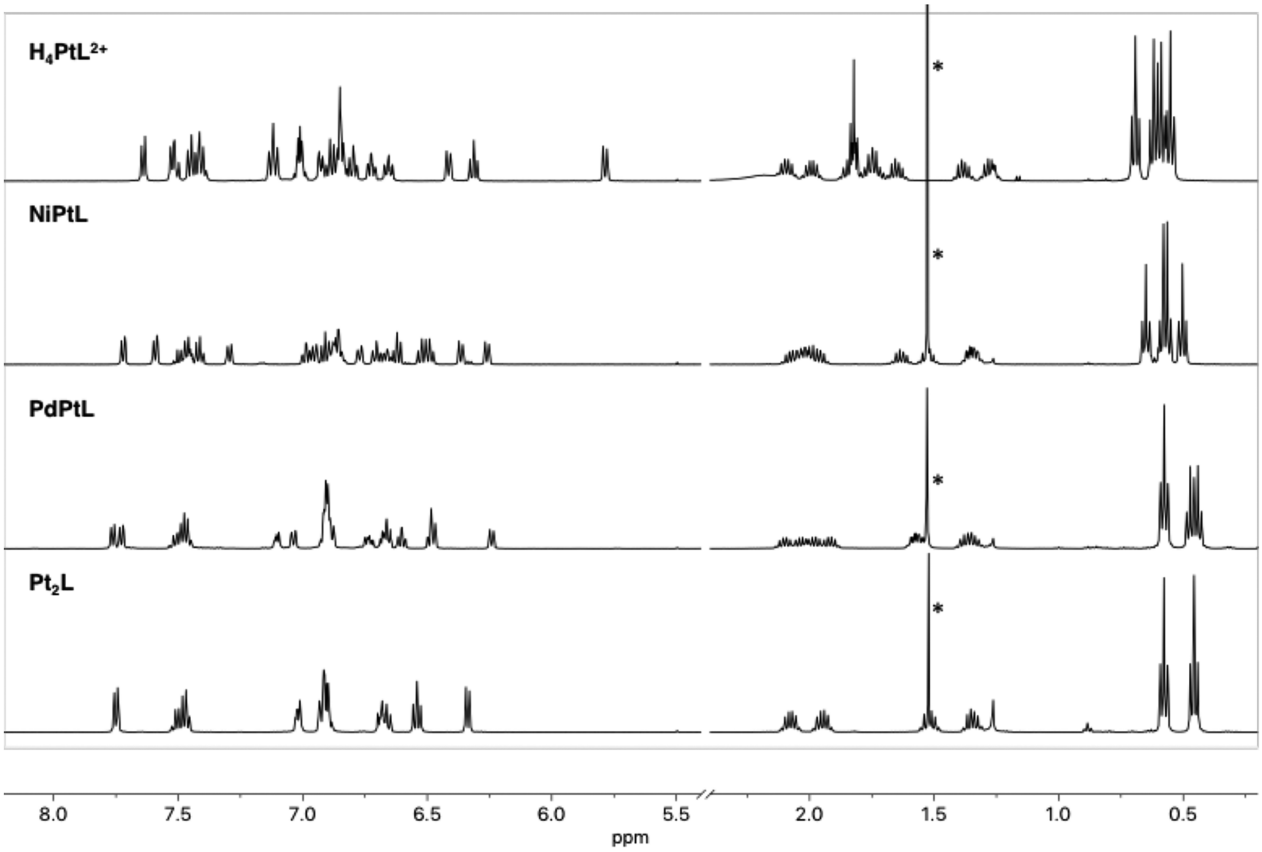

Figure 3. (A) Stacked ^{1}H NMR spectra (500 MHz, CD_2Cl_2, 298 K): **H_2PtL** + 2 equiv of TFA (**H_3PtL$^+$** and **H_4PtL^{2+}**), **NiPtL**, **PdPtL**, and **Pt_2L**. The downfield NH signals for **H_2PtL** + 2 equiv of TFA are not shown (see the Supporting Information). Asterisks indicate H_2O.

tetrapyrroles, with molar extinction coefficients (ε) between 6 $\times 10^4$ and 8 $\times 10^4$ M^{-1} cm^{-1}. The absence of any significant extension of the UV−vis absorbance into the NIR, as is frequently observed in aromatic expanded porphyrins,[63] also reflects the lack of continuous macrocycle π conjugation of the group 10 metal complexes of the twin porphyrin (Figure 4).

The UV−vis spectrum of the free base ligand **H_4L** exhibits two intense bands at 390 and 638 nm with a shoulder on the longest-wavelength band (λ_{max}). Upon complexation with one metal ion, three primary bands arise with some additional minor features present. The monometallic species **H_2PtL** absorbs well into the NIR, with the λ_{max} band tailing past 1000 nm. The spectrum of the homobimetallic complex **Pd_2L** possesses three intense and sharpened bands, similar to those observed for the corresponding **Ni_2L** complex. The UV−vis spectrum of **Pt_2L** is much different and most striking in its complexity in the range between 250 and 550 nm. Furthermore, its Q-like band region with λ_{max} at 768 nm has the longest wavelength of all of the bimetallic twin porphyrin complexes thus prepared. The heterobimetallic complexes exhibit UV−vis absorbances that are intermediate between the parent homobimetallic species. The Pt-based complexes **NiPtL** and **PdPtL**, for example, reflect the complexities seen in the spectrum of **Pt_2L**, albeit much less pronounced.

Monometallic **H_2PtL** can be reversibly protonated with TFA to obtain the monoprotonated **H_3PtL$^+$** and diprotonated **H_4PtL^{2+}** species. The three main absorbance bands ultimately become hypsochromically shifted, with each band blue-shifting 26−52 nm from the initial neutral to final diprotonated species (see the Supporting Information), reminiscent of the **H_2PdL** titration series.[34]

Electrochemistry. All bimetallic complexes were studied using cyclic voltammetry (CV), exhibiting one electrochemically quasi-reversible reduction ($E^{red}_{1/2}$ = −1.901 to −1.79 V vs $Fc^{+/0}$) and two quasi-reversible oxidations ($E^{ox1}_{1/2}$ = −0.119 to −0.032 V and $E^{ox2}_{1/2}$ = +0.374 to +0.447 V vs $Fc^{+/0}$; Figure 5 and Table 2). **Pt_2L** is most easily oxidized to [**Pt_2L**]$^+$, followed by oxidation of **Ni_2L** to [**Ni_2L**]$^+$, and last of**Pd_2L** to [**Pd_2L**]$^+$ ($E^{ox1}_{1/2}$ = −0.104, −0.05, and −0.032 V vs $Fc^{+/0}$, respectively). Likewise, the first oxidation potential in the heterobimetallic series follows the sequence [**NiPtL**]$^+$ < [**NiPdL**]$^+$ < [**PdPtL**]$^+$ ($E^{ox1}_{1/2}$ = −0.119, −0.073, and −0.063 V vs $Fc^{+/0}$, respectively). Past studies of **Ni_2L**, **NiCuL**, **Cu_2L**, and **H_2PdL** indicated that the chemically reversible and electrochemically quasi-reversible oxidative processes were ligand-centered.[34,41,42] Consistent with trends observed in the past, the redox potentials observed here change little with the type of group 10 d^8 metal ion, suggesting that ligand-centered redox events are also involved. The cyclic voltammogram of the monometallic **H_2PtL** complex shows only one quasi-reversible reduction ($E^{red}_{1/2}$ = −1.482 V vs $Fc^{+/0}$) and one quasi-reversible oxidation ($E^{ox}_{1/2}$ = −0.231 V vs $Fc^{+/0}$), as was also observed for its Pd^{II} analogue **H_2PdL** ($E^{red}_{1/2}$ = −1.59 V and $E^{ox}_{1/2}$ = −0.32 V vs $Fc^{+/0}$).[34] We infer from this that the single-electron-oxidized species of **H_2PtL** is also a ligand-centered π-cation radical confined to the metalated side of the macrocycle, while the π-anion radical is located on the nonmetalated side.[34] As reported previously, the **H_2NiL** complex did not display any reversible redox events.[42]

https://dx.doi.org/10.1021/acs.inorgchem.0c00714
Inorg. Chem. XXXX, XXX, XXX−XXX

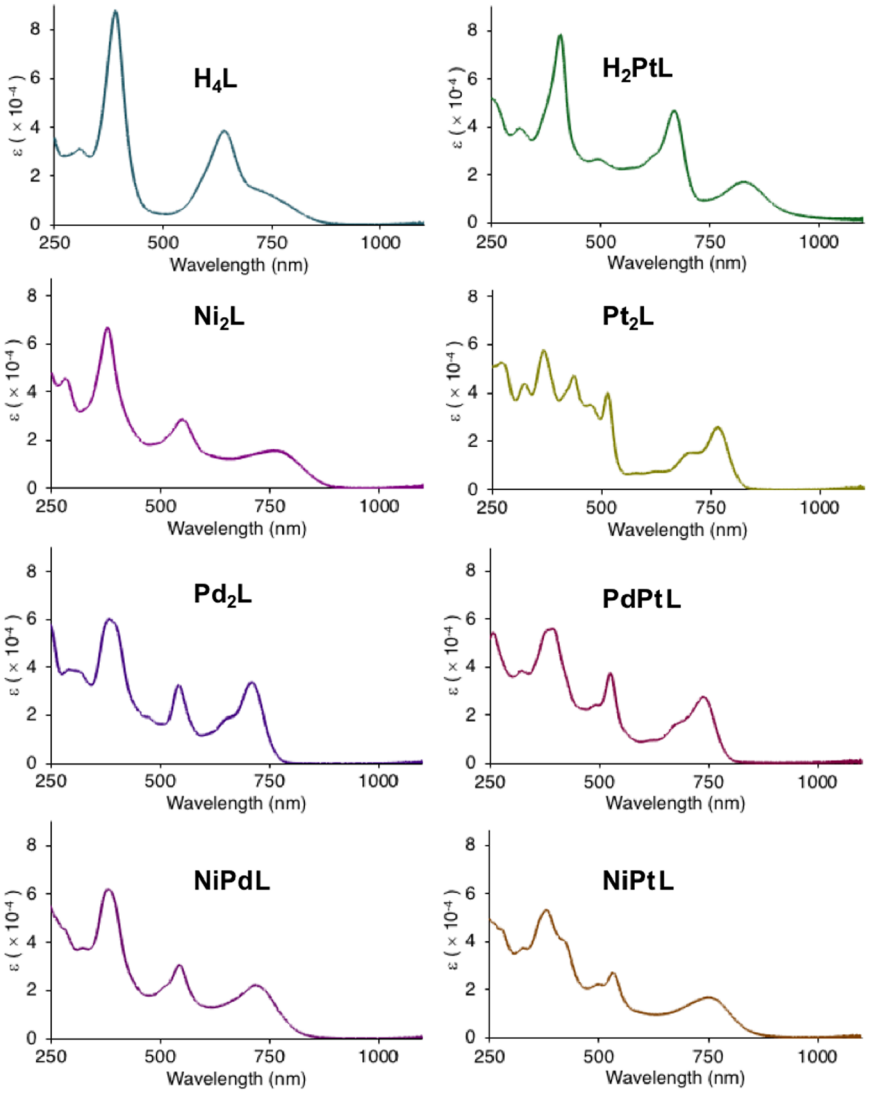

Figure 4. UV−vis spectra (CH_2Cl_2) of the compounds indicated.

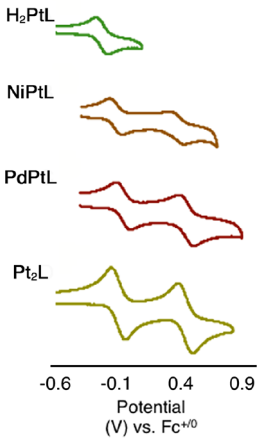

Figure 5. Cyclic voltammograms (CH_2Cl_2, 0.1 M NBu_4PF_6, at 100 mV s^{-1}) of the compounds indicated. See the Supporting Information for the scans toward negative potentials.

The comproportionation constants (K_c) calculated based on $\Delta E^{ox}_{1/2}$ ($\Delta E^{ox}_{1/2} = E^{ox2}_{1/2} - E^{ox1}_{1/2}$) are 10^7 for **Ni_2L** and **Pd_2L** and higher, 10^9, for **Pt_2L**. The heterobimetallic complexes fall between their respective homobimetallic complexes and are 10^7 for **NiPdL** and 10^8 for **NiPtL** and **PdPtL**. These numbers provide some insight into the thermodynamic stability of the singly oxidized Pt^{II}-containing complexes relative to complexes of the lighter group 10 metal ions, which is likely correlated to charge delocalization effects.[64]

Table 2. Selected Redox Parameters (Potentials vs $Fc^{+/0}$)

	$E^{red}_{1/2}$ (V)	$E^{ox1}_{1/2}$ (V)	$E^{ox2}_{1/2}$ (V)	**ox_1-red** (V)	**ox_2-ox_1** (V)
Ni_2L[a]	−1.79	−0.05	+0.41	1.74	0.46
Pd_2L	−1.825	−0.032	+0.439	1.793	0.471
Pt_2L	−1.898	−0.104	+0.438	1.794	0.542
NiPdL	−1.864	−0.073	+0.383	1.791	0.456
NiPtL	−1.901	−0.119	+0.374	1.782	0.493
PdPtL	−1.866	−0.063	+0.447	1.803	0.510
H_2PtL	−1.482	−0.231		1.251	
H_2PdL[b]	−1.59	−0.32		1.27	

[a]Reference 42. [b]Reference 34.

Spectroelectrochemistry. Spectroelectrochemical studies confirm the chemical reversibility of the species upon oxidation and rereduction by comparing the initial and final UV−vis−NIR spectra. In addition, the UV−vis−NIR absorbance spectra

https://dx.doi.org/10.1021/acs.inorgchem.0c00714
Inorg. Chem. XXXX, XXX, XXX−XXX

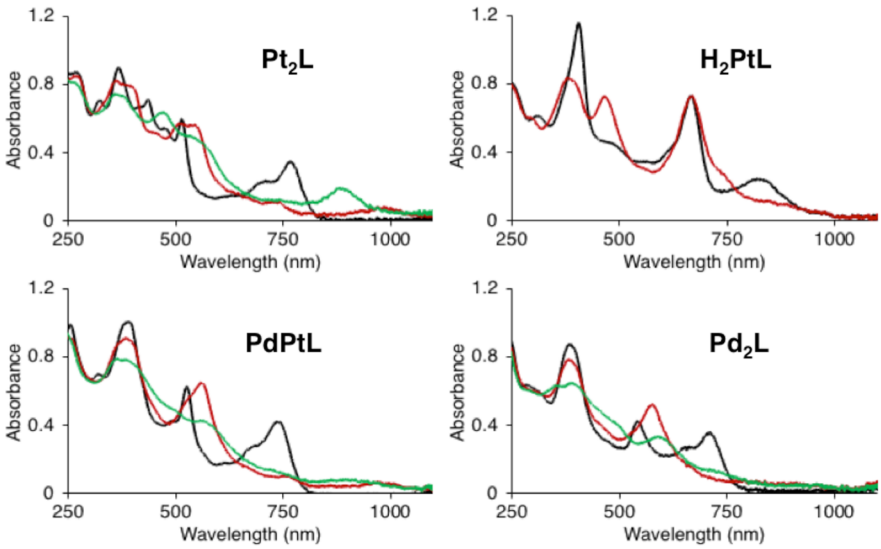

Figure 6. Spectroelectrochemical traces (CH_2Cl_2, 0.1 M NBu_4PF_6) of the compounds indicated. Black traces correspond to the neutral species, red traces to the singly oxidized species, and green traces to the doubly oxidized species.

of once- and twice-oxidized species can also be determined. Features such as increased absorbance in the NIR region are indicative of the formation of ligand-centered cation radical species, as was also shown before for **H_2NiL** (Figure 6).[42]

MCD. The MCD spectra and corresponding UV−vis spectra of the compounds investigated are shown in Figure 7 (cf. also to Figure 4). The MCD spectrum of the **H_4L** free-base ligand consists of rather weak Faraday *B* terms, with the most intense negative signal in the visible region centered at 686 nm, which does not correlate to any of the major absorption peaks in the UV−vis spectrum. In the higher energy region, the MCD spectrum revealed three negative signals at 533, 421, and 365 nm and two positive Faraday MCD *B* terms observed at 459 and 327 nm, which again do not correlate with the energy of the intense absorption band observed at 390 nm in the UV−vis spectrum of **H_4L**.

For monometallic **H_2ML** complexes, the relatively strong bands at 683 nm (**H_2NiL**), 662 nm (**H_2PdL**), and 664 nm (**H_2PtL**) in the visible region are complemented by a fingerprint NIR band between 797 and 829 nm unique to the monometallic twin porphyrin complexes. Unlike in the case of **H_4L**, no spectral absorption gap was observed between the UV and visible portions of their optical spectra. The MCD spectra of the monometallic derivatives are dominated by a negative signal centered between 481 and 566 nm for **H_2NiL** and a broad band around 550 nm observed for both **H_2PdL** and **H_2PtL**. The NIR fingerprint bands of the monometallic twin porphyrins are associated with weak and positive Faraday *B* terms: one for **H_2NiL** and two each for **H_2PdL** and **H_2PtL**. Similar to the metal-free twin porphyrin, the two most intense absorption bands in the UV−vis spectra of the monometallic derivatives do not show much MCD intensity. The NIR band observed in the absorption spectra for the monometallic derivatives disappears in the case of both homobimetallic and heterobimetallic complexes. Indeed, in the case of the bimetallic compounds, the low-energy spectral envelope is dominated by a prominent band observed between 709 and 767 nm; the bimetallic complexes possess a fingerprint band located between 514 and 548 nm. In all bimetallic complexes, the low-energy visible or NIR MCD signals have negative intensities and do not correlate with the most intense bands observed in the UV−vis spectra of these compounds.

Thus, in all cases, the most intense absorption bands in the UV−vis spectra of the metal-free, monometallic, and bimetallic twin porphyrins do not possess much MCD intensity. This is in strong contrast to the intense MCD signals that are observed for the Q and Soret bands of metal-free and transition-metal metalloporphyrins and many of their analogues.[65−69] As was pointed out earlier for the homobimetallic Cu^{II} twin porphyrin complex,[41] the low intensity of the MCD signals is associated with pure macrocycle-centered $\pi-\pi^*$ excitations and likely reflects their twisted, nonplanar geometries and poor overlap between atomic π orbitals, resulting in a lack of any strong and delocalized macrocyclic ring current. Thus, their low-intensity MCD transitions indicate that the twin porphyrin π system behaves more like an open-chain tetrapyrrole and not like an aromatic macrocyclic porphyrinic compound. Indeed, the highly nonplanar structure of the twin porphyrins incorporating two nearly independent π systems is one of their defining characteristics.[32,34,42] Low-intensity MCD spectra were also observed for other macrocyclic porphyrinoids with compromised ~~or~~ localized π-aromatic systems.[70]

DFT and TDDFT. To better correlate the spectroscopic properties observed for the metal-free, monometallic, and bimetallic twin porphyrin complexes, the electronic structures of selected compounds were evaluated using DFT and TDDFT calculations. The resulting molecular orbital (MO) energy diagram is shown in Figure 8.

For all compounds, the highest occupied molecular orbital (HOMO) and HOMO−1 orbitals as well as the lowest unoccupied molecular orbital (LUMO) and LUMO+1 orbitals are energetically well separated from the remaining filled or empty orbitals, respectively. The HOMO to HOMO−1 as well as LUMO to LUMO+1 energy gaps decrease in the order of **H_2NiL** > **H_2PdL** > **H_4L**, while similar gaps for the bimetallic **Ni_2L**, **Pd_2L**, and **NiPdL** complexes were predicted to be close to each other.

While the HOMO orbitals of the free base as well as the homobimetallic and heterobimetallic complexes are evenly

https://dx.doi.org/10.1021/acs.inorgchem.0c00714
Inorg. Chem. XXXX, XXX, XXX−XXX

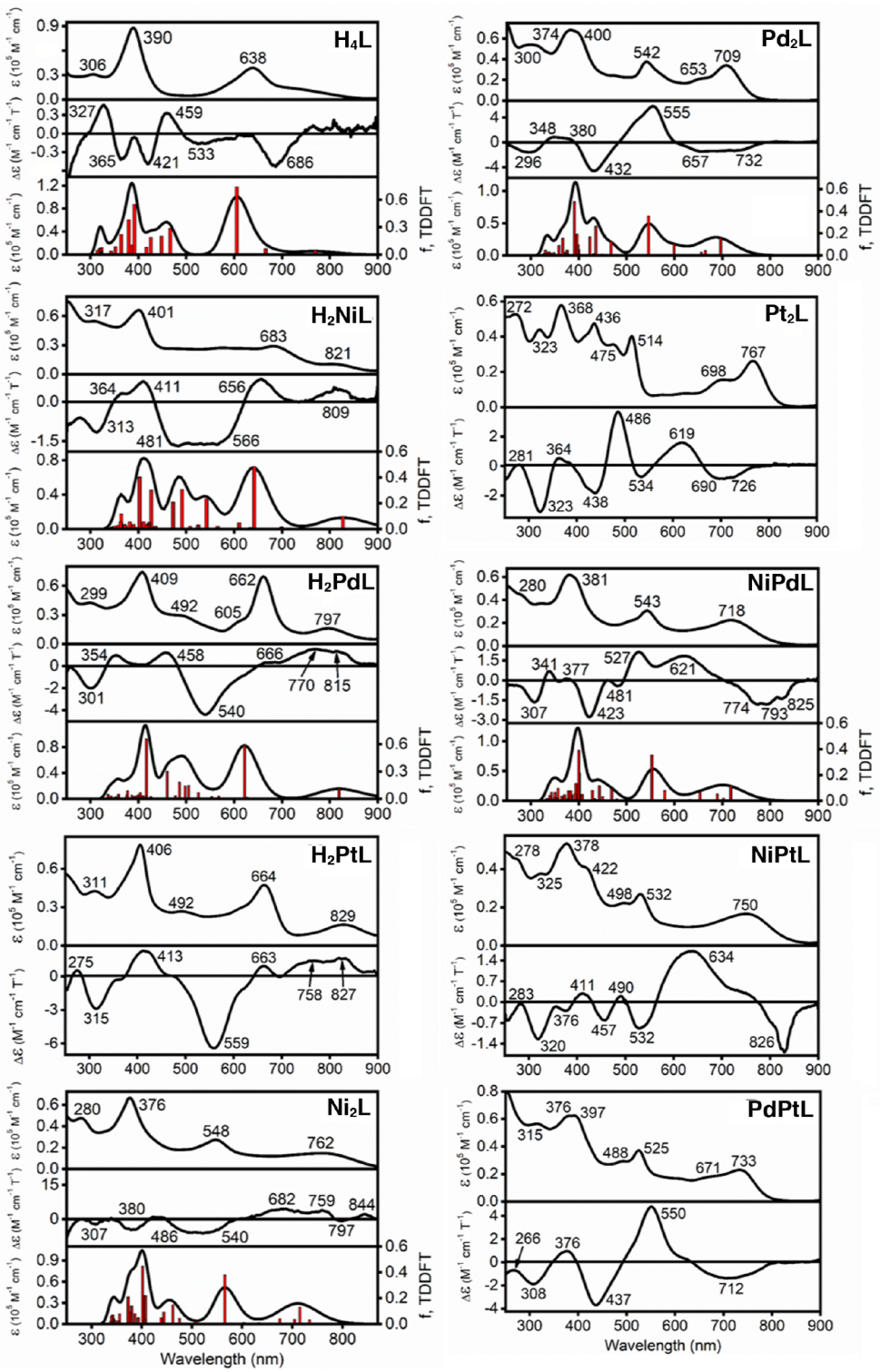

Figure 7. UV−vis (top), MCD (middle), and TDDFT-predicted (bottom) spectra of target compounds (all in CH_2Cl_2). Only the UV−vis (top) and MCD (bottom) spectra of the Pt^{II} complexes are shown.

distributed over the macrocycle, they are mostly centered on the metalated halves of the molecule in the monometallic species (Figure 9 and the Supporting Information). The LUMO orbitals in **H_2NiL** and **H_2PdL** are localized on the metal-free part of the macrocycle. The LUMO+1 and LUMO +2 orbitals of **H_2NiL** are close in energy, with the former localized over the metal-free part and the latter over the metal-containing part of the macrocycle. In comparison, the LUMO +1 and LUMO+2 orbitals of **H_2PdL** are better separated and feature an inverse localization.

A MO composition analysis further refines this picture (Figure 10), revealing that the contribution of the pyrazole fragments to the frontier orbitals of all compounds does not exceed 25%, while the contributions from the pyrrolic

https://dx.doi.org/10.1021/acs.inorgchem.0c00714
Inorg. Chem. XXXX, XXX, XXX−XXX

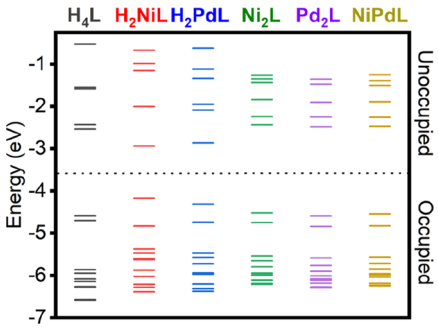

Figure 8. DFT-predicted frontier orbital energy diagram for the compounds indicated.

fragments to the HOMO−1 to LUMO+1 MOs play a dominant role. In the case of the monometallic and bimetallic compounds, the contribution from the transition-metal orbitals to the frontier MOs does not exceed 10%.

The nature of the excited states in all Ni- and Pd-containing compounds was probed by TDDFT calculations (Figure 7). In all cases, reasonable agreement between theory and experiment was observed. Specifically in the case of the metal-free twin porphyrin **H_4L**, the energy of the experimentally observed features between 700 and 800 nm in the UV−vis spectrum correlates well with the energy of the first excited state, predicted at 769 nm and characterized as a pure HOMO → LUMO single-electron transition that is predominantly centered at pyrrolic fragments of the twin porphyrin core. The TDDFT calculations suggest that the relatively intense MCD signal observed at 686 nm represents the third excited state predicted at 666 nm, which is dominated by the HOMO−1 → LUMO+1 single-electron excitation. TDDFT calculations also predict that the most intense transition, experimentally observed at 638 nm (predicted at 605 nm), is dominated by a nearly equal contribution from the HOMO−1 → LUMO and HOMO → LUMO+1 single-electron excitations (fourth excited state). The predicted higher energy of the 4th excited state compared to that of the 3rd excited state, is rationalized by the configuration interaction between the energetically similar HOMO/HOMO−1 and LUMO/LUMO+1 orbitals. The most intense transition in the higher-energy region observed at 390 nm is associated with nearly equal HOMO−3 → LUMO+1 and HOMO−6 → LUMO single-electron excitations (excited state 14). The latter single-electron excitation has a distinct pyrazole(π) → pyrrole(π^*) charge-transfer character.

In the case of the monometallic **H_2NiL** and **H_2PdL** complexes, TDDFT calculations correctly predicted a hypsochromic shift of the lowest energy NIR band when shifting from the lighter to the heavier metal ion, as well as a hypsochromic shift of the most prominent visible band (observed at 683 nm in **H_2NiL** and 662 nm in **H_2PdL**) and a bathochromic shift of the most prominent band observed at ∼400 nm. The first NIR band, observed at ∼800 nm, is predominantly associated with the HOMO−1 → LUMO single-electron excitation, while the intense band in the visible region observed between 660 and 680 nm for these compounds is predicted to be dominated by the HOMO → LUMO+2 (**H_2NiL**) or HOMO → LUMO+1 (**H_2PdL**) single-electron excitations. Similar to the metal-free twin porphyrin

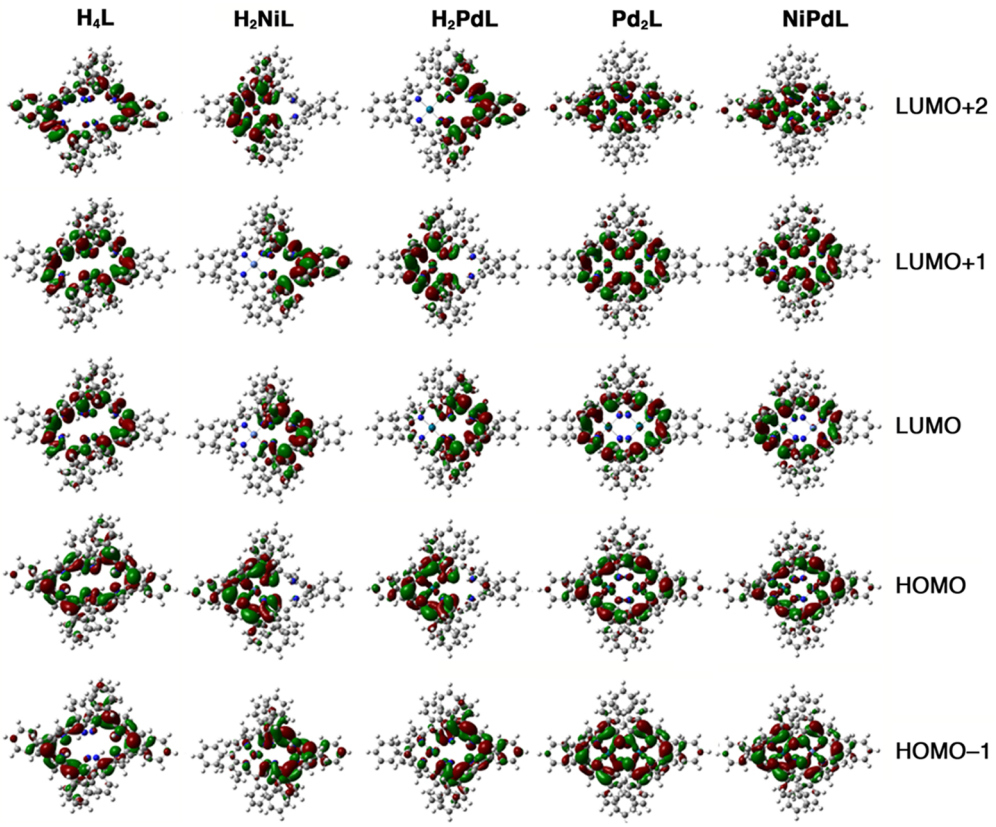

Figure 9. DFT-predicted frontier orbitals for the compounds indicated. See the Supporting Information for the frontier orbitals of the full set of compounds investigated.

https://dx.doi.org/10.1021/acs.inorgchem.0c00714
Inorg. Chem. XXXX, XXX, XXX−XXX

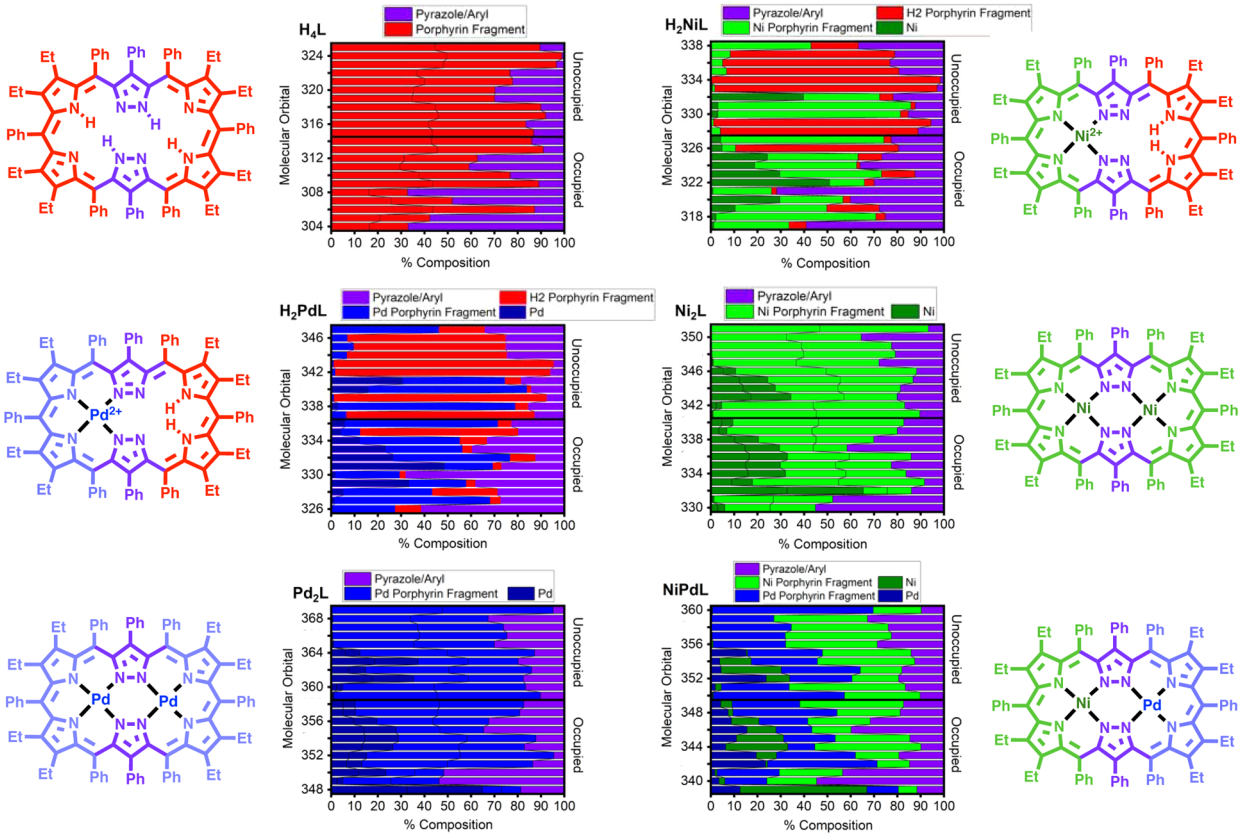

Figure 10. DFT-predicted frontier orbital compositions for the compounds indicated.

H_4L, the intense transition observed at ∼400 nm was predicted to have a substantial pyrazole(π) → pyrrole(π^*) intramolecular charge-transfer character. Importantly, the TDDFT calculations correctly predicted an energy gap at ∼480 nm, which was experimentally observed in the UV−vis spectrum of **H_4L** but is filled with numerous excited states in the **H_2NiL** and **H_2PdL** complexes.

Three distinct absorption envelopes were predicted for the bimetallic **Ni_2L**, **Pd_2L**, and **NiPdL** twin porphyrin complexes without any spectral gap between the UV and visible parts in the spectra of these compounds, in full agreement with experimental observations. In all cases, the intense NIR absorption is dominated by the HOMO → LUMO single-electron excitation centered at the pyrrolic π and π^* orbitals. The most intense absorption band in the visible region of the absorption spectrum for these compounds observed around 545 nm correlates well with the TDDFT-predicted excited state at 550 nm, which is dominated by the HOMO−1 → LUMO+1 single-electron excitations centered at the pyrrolic π and π^* orbitals. Parallel to the free-base and monometallic cases, the most intense absorption band in the higher-energy region (∼400 nm) correlates well with an excited state dominated by a single-electron transition with significant pyrazole(π) → pyrrole(π^*) intramolecular charge-transfer character.

Overall, it appears that the TDDFT calculations correctly predict the broad spectral nature of the monometallic and bimetallic twin porphyrin complexes and accurately predict general trends observed in the UV−vis spectra of these compounds to within ∼0.1 eV error, which is typical for modern TDDFT methods.[71−73] A large number of TDDFT transitions in all target compounds correlate well with the complex MCD spectra of these systems, indicative of a large number of excited states observed in the UV−vis-to-NIR spectral envelope.

■ CONCLUSIONS

A comprehensive series of group 10 complexes of the twin porphyrin **H_4L**, including the first Pt^{II}-containing complexes **H_2PtL** and **Pt_2L** as well as the novel heterobimetallic complexes **NiPdL**, **NiPtL**, and **PdPtL**, were prepared and analyzed. Structurally, the bimetallic complexes do not differ considerably from each other or from related twin porphyrin complexes reported previously.[19,32−34] The diamagnetic nature of the complexes hosting low-spin d^8 group 10 metal ions allowed a comparison of their well-resolved NMR spectra. The quasi-reversible oxidative and reductive processes observed for the bimetallic species show only subtle variations for the different metal ions, supporting the mostly ligand-centered nature of these redox events. In contrast, their optical spectra are distinctly different from each other, indicative of a mixing of the d orbitals of the metal ions with the π system of the ligand. The low MCD intensity of the group 10 metal complexes of twin porphyrin **H_4L** stands in contrast to the generally intense MCD signals for the Q and Soret bands of transition-metal metalloporphyrins, but the finding is in line with the absence of a strong macrocyclic ring current. This confirms previous notions that the highly twisted twin porphyrin does not possess macrocyclic aromatic character but features two nearly independent conjugated π systems that are separated by the central pyrazolate units.[19,32−34]

(TD)DFT calculations allowed further analysis of the rich UV−vis to NIR spectral features of the monometallic and

https://dx.doi.org/10.1021/acs.inorgchem.0c00714
Inorg. Chem. XXXX, XXX, XXX−XXX

bimetallic twin porphyrin complexes. The frontier MOs involved in the lowest energy transitions are predominantly located at the pyrrolic fragments of the twin porphyrin core, with only minor contributions of the pyrazole units (<25%) and group 10 metal ions (<10%). While frontier orbitals extend over the entire macrocycle for the homobimetallic and heterobimetallic complexes, monometalation results in the HOMO being confined to the metalated half and the LUMO being confined to the free-base half. The panchromatic absorbance of the twin porphyrin complexes, in conjunction with their electrochemical and spectroelectrochemical signatures, suggests that these systems may find utility in optoelectronic or electrochromic applications.

■ EXPERIMENTAL SECTION

Materials. Solvents were of reagent-grade or better and were used as received, except CH_2Cl_2 for electrochemistry and spectroelectrochemistry, which was passed over activated silica gel and degassed under Ar. Chromatography: silica gel for column chromatography (technical grade, 60 Å, 70−230 mesh, 63−200 μm, Aldrich); aluminum-backed silica gel TLC plates (60 F_{254}, Merck Millipore), neutral and basic alumina 90 for column chromatography (Machery-Nagel), and neutral aluminum oxide TLC plates (0.2 mm, thickness, with 254 nm indicator, Fluka) were used.

H_4L,[19,32,40] **H_2NiL**,[42] **H_2PdL**,[34] and **Ni_2L**[32,42] were prepared according to literature procedures with slight modifications, as detailed in the Supporting Information. All reactions were shielded from light by covering the reaction flask with aluminum foil.

Instruments. NMR spectra (^{1}H, ^{13}C, ^{195}Pt, and 2D) were recorded in CD_2Cl_2 on a Bruker Avance 500 MHz spectrometer at 298 K. Acid titrations were conducted at 268 K on a Bruker Avance 400 MHz spectrometer. High-resolution mass spectrometry was performed by the Central Analytics Laboratory at the Georg-August-Universität Göttingen using a ThermoFisher LTQ Orbitrap XL mass spectrometer. UV−vis spectra were collected using an Agilent Cary 60 UV−vis spectrophotometer at ambient temperature.

CV. Voltammograms were obtained from 10^{-3} M twin porphyrin complexes in 0.1 M tetrabutylammonium hexafluorophosphate (NBu_4PF_6) in an anhydrous CH_2Cl_2 solution using a PerkinElmer 263A potentiostat with a glassy carbon working electrode, a Pt wire counter electrode, and a Ag wire reference electrode, with decamethylferrocene [$(Cp^*)_2Fe$] as the internal standard (see additional details for conversion in the Supporting Information).

Spectroelectrochemistry. Measurements were performed in CH_2Cl_2/0.1 M NBu_4PF_6 under ambient conditions using a Metrohm Autolab PGSTAT101 potentiostat coupled with an Avantes AvaLight DH-S-BAL light source and an Avantes StarLine AvaSpec-2048 fiber-optic spectrometer equipped with *Nova* and *AvaSoft* software following a chronoamperometry protocol (spectra recorded between 250 and 1100 nm). A Pt mesh working electrode, a Pt wire counter electrode, and a freshly prepared Ag/$AgNO_3$ (10 mM $AgNO_3$/100 mM NBu_4PF_6/MeCN) reference electrode were used.

X-ray Diffractometry. Crystals suitable for X-ray diffractometry were grown under ambient conditions. Solvent layering of CH_2Cl_2 with MeOH produced X-ray-quality crystals of **Pt_2L**, vapor diffusion of MeOH into $CHCl_3$ (EtOH-stabilized; passed over K_2CO_3 before use) resulted in **NiPdL** and **NiPtL** crystals, and vapor diffusion of MeOH into CH_2Cl_2/$CHCl_3$ produced **PdPtL** crystals. For experimental details, see the Supporting Information.

UV−Vis/MCD Spectroscopy. All UV−vis spectra were collected on a Jasco V-770 spectrophotometer (CH_2Cl_2), and MCD spectra were measured (CH_2Cl_2) with a Jasco J-1500 CD spectrometer using a Jasco MCD-581 electromagnet operated at 1.0 T. The MCD spectra were recorded in mdeg = [θ] and converted to molar ellipticity as $\Delta\varepsilon = \theta/(32980Blc)$, where B is the magnetic field, l is the path length (cm), and c is the concentration (M).[74] The MCD spectra were measured at 10 °C in parallel and antiparallel orientations with respect to the magnetic field.

DFT and TDDFT Methods. All calculations were performed using the *Gaussian 09* software package[75] on UNIX OS. The geometries of all twin porphyrins were optimized using the hybrid B3LYP exchange-correlation functional[76] and full-electron DGDZVP basis set[77] in the gas phase. Frequency calculations were run to ensure that a global energetic minimum on the potential energy surface was obtained. The optimized geometries were used for single-point and TDDFT calculations. The 60 lowest-energy excited states were considered for TDDFT calculations. Only Ni and Pd complexes were modeled using DFT and TDDFT methods because of the lack of a DGDZVP basis set for the Pt ion.

Homobimetallic Pd^{II} Complex, Pd_2L. The free base **H_4L** (17.9 mg, 13.75 μmol) was dissolved in $C_2H_4Cl_2$-1,2 (4 mL). Palladium(II) acetate [$Pd(OAc)_2$; 8.9 mg, 39.7 μmol, 2.8 equiv] dissolved in $C_2H_4Cl_2$-1,2 (2 mL) was added, and the solution was brought to reflux for 1 h or until the teal starting material was consumed and formation of the nonpolar purple **Pd_2L** was observed (using TLC, silica−1:2 hexane/EtOAc). The solvent was removed by rotary evaporation, and the residue was purified using column chromatography. Collection of the nonpolar purple fraction, solvent removal by rotary evaporation, and then recrystallization from THF layered with MeOH for a few days at 0 °C yielded dark-purple microcrystalline material (13.2 mg, 63%). R_f = 0.90 (silica−2:1 hexane/EtOAc). ^{1}H NMR (500 MHz, CD_2Cl_2, 298 K): δ 7.73 (dt, J = 6.6 Hz, 4H, Ph^A), 7.50 (dt, J = 6.7 Hz, 2H, Ph^A), 7.47 (m, 4H, Ph^A), 7.01 (m, 4H, Ph^B), 6.99 (m, 4H, Ph^B), 6.90 (m, 8H, Ph^B), 6.72 (m, 4H, Ph^B), 6.66 (tt, J = 7.4 Hz, 2H, Ph^C), 6.54 (t, J = 7.5 Hz, 4H, Ph^C), 6.38 (d, J = 6.9 Hz, 4H, Ph^C), 2.06 (sextet, J = 7.3 Hz, 4H, $^aCH_2$), 1.95 (sextet, J = 7.3 Hz, 4H, $^bCH_2$), 1.63 (sextet, J = 7.3 Hz, 4H, $^bCH_2$), 1.36 (sextet, J = 7.4 Hz, 4H, $^aCH_2$), 0.58 (t, J = 7.4 Hz, 12H, $^aCH_3$), 0.46 (t, J = 7.3 Hz, 12H, $^bCH_3$). ^{13}C NMR (125 MHz, CD_2Cl_2, 298 K): δ 157.2 (α-pyrr-a), 152.5 (3/5-Pz), 147.7 (β-pyrr-b), 147.2 (α-pyrr-b), 145.6 (β-pyrr-a), 139.6 (*ipso*-Ph^A), 137.4 (*ipso*-Ph^B), 134.5 (Ph^A), 134.1 (*ipso*-Ph^C), 133.8 (Ph^B), 132.6 (Ph^C), 132.0 (Ph^B), 128.5 (Ph^A), 128.2 (Ph^A), 127.7 (Ph^B), 127.6 (Ph^B), 127.0 (Ph^B), 126.9 (Ph^C), 125.3 (Ph^C), 124.8 (*meso*-Ph^C), 123.7 (*meso*-Ph^B), 110.3 (*meso*-Ph^A), 19.6 ($^bCH_2$), 19.3 ($^aCH_2$), 16.2 ($^aCH_3$), 15.7 ($^bCH_3$). For details of the ^{1}H and ^{13}C NMR assignments, see the Supporting Information. UV−vis [CH_2Cl_2; λ_{max}, nm (ε, M^{-1} cm^{-1})]: 709 (34000), 654 (19200, shoulder), 542 (32800), 472 (19700), 383 (60500), 314 (38700), 300 (39100). HR-MS (ESI$^+$, CH_2Cl_2/CH_3CN): m/z 1510.4603 (calcd m/z 1510.4610 for $C_{92}H_{80}N_8Pd_2^+$).

Homobimetallic Pt^{II} Complex, Pt_2L. The free base **H_4L** (34.7 mg, 26.7 μmol) was dissolved in $C_2H_4Cl_2$-1,2 (12 mL), and then CH_3CN (8 mL) was added while the solution was warmed. PtI_2 (64.8 mg, 144 μmol, 5.4 equiv) and NaOAc·$3H_2O$ (21.8 mg, 160 μmol, 6.0 equiv) were added to the warm solution and brought to reflux for 8 h or until teal **H_4L** was consumed and nonpolar yellow-green **Pt_2L** formed (monitored by TLC). The volume of the reaction mixture was reduced and submitted to column chromatography (silica−hexane/CH_2Cl_2). Solvent removal from the nonpolar olive-green fraction and recrystallization of the residue from THF layered with MeOH at 0 °C resulted in crystalline **Pt_2L** (12.0 mg, 27%). R_f = 0.88 (silica−2:1 hexane/EtOAc). ^{1}H NMR (500 MHz, CD_2Cl_2, 298 K): δ 7.75 (dt, J = 6.2 Hz, 4H, Ph^A), 7.51−7.47 (m, 6H, Ph^A), 7.01 (m, 4H, Ph^B), 6.91 (m, 12H, Ph^B), 6.68 (m, 6H, Ph^B/Ph^C), 6.54 (t, J = 7.7 Hz, 4H, Ph^C), 6.34 (d, J = 6.8 Hz, 4H, Ph^C), 2.08 (sextet, J = 7.4 Hz, 4H, $^aCH_2$), 1.94 (sextet, J = 7.3 Hz, 4H, $^bCH_2$), 1.53 (sextet, J = 7.4 Hz, 4H, $^bCH_2$), 1.35 (sextet, J = 7.3 Hz, 4H, $^aCH_2$), 0.58 (t, J = 7.3 Hz, 12H, $^aCH_3$), 0.46 (t, J = 7.3 Hz, 12H, $^bCH_3$). ^{13}C NMR (125 MHz, CD_2Cl_2, 298 K): δ 152.7 (C_q), 148.7 (C_q), 146.6 (C_q), 145.4 (C_q), 144.1 (C_q), 139.3 (C_q), 137.0 (C_q), 134.8 (Ph^A), 134.1 (C_q), 133.9 (Ph^B), 133.4 (Ph^C), 132.1 (Ph^B), 128.6 (Ph^A), 128.1 (Ph^A), 127.6 (Ph^B), 127.4 (Ph^B), 127.0 (2 × intensity Ph^C), 125.4 (Ph^C), 122.4 (C_q), 108.6 (C_q), 19.8 ($^bCH_2$), 19.4 ($^aCH_2$), 16.4 ($^aCH_3$), 15.7 ($^bCH_3$). For details of the ^{1}H and ^{13}C NMR assignments, see the Supporting Information; broad peaks in the HMBC spectrum limit assignments of quaternary C atoms. ^{195}Pt NMR (107 MHz, CD_2Cl_2, 298 K): δ −2437. UV−vis [CH_2Cl_2; λ_{max}, nm (ε, M^{-1} cm^{-1})]: 768 (26200), 709 (15500), 515 (39900), 476 (35300), 437 (47000), 417

https://dx.doi.org/10.1021/acs.inorgchem.0c00714
Inorg. Chem. XXXX, XXX, XXX−XXX

(39900), 368 (57400), 323 (43800), 272 (52500). HR-MS (ESI$^+$, CH_2Cl_2/CH_3CN): m/z 1687.5795 (calcd m/z 1687.5817 for $C_{92}H_{80}N_8Pt_2^+$).

Monometallic Pt^{II} Complex, H_2PtL. The reaction conditions described for **Pt_2L** were optimized to afford **H_2PtL** as the main product using **H_4L** (74.0 mg, 56.8 μmol), PtI_2 (83.3 mg, 186 μmol, 3.3 equiv), and $NaOAc{\cdot}3H_2O$ (19.1 mg, 140 μmol, 2.5 equiv) in a mixed solvent system (24 mL of $C_2H_4Cl_2$-1,2 and 16 mL of CH_3CN) to improve the solubility and then brought to reflux for 4 h. The solvent was removed under vacuum, followed by purification using column chromatography, and then solvent removal and recrystallization to afford crystalline **H_2PtL** (18.2 mg, 21%). R_f = 0.62 (silica−2:1 hexane/EtOAc). Typically <5% crystalline **Pt_2L** was also obtained. UV−vis [CH_2Cl_2; λ, nm (ε, M^{-1} cm^{-1})]: 825 (17000), 667 (46700), 617 (27800), 494 (26500), 406 (78500), 315 (39200). ^{1}H NMR (500 MHz, CD_2Cl_2, 298 K): δ 7.47−7.65 (m, 2H), 7.42−7.39 (m, 4H), 6.99−6.92 (m, 12H), 6.75 (m, 3H), 6.64−6.61 (m, 6H), 6.55−6.50 (m, 5H), 6.32 (br s, 2H), 5.77 (br s, 2H), 3.68 (t, 3H), 2.11−2.04 (m, 4H), 1.90−1.80 (overlapping m, 10H), 1.36−1.28 (m, 4H), 0.74 (t, J = 7.5 Hz, 6H), 0.64 (t, J = 7.5 Hz, 6H), 0.68−0.58 (m, 12H). ^{13}C NMR (125 MHz, CD_2Cl_2, 298 K): δ 155.9, 148.8, 142.5, 137.5, 133.7, 131.5, 130.7, 128.7, 128.6, 128.5, 127.9, 127.5, 127.2, 127.0, 126.3, 126.6, 126.1, 124.5, 68.2, 26.0 (CH_2), 19.1 (CH_2), 18.8 (CH_2), 18.6 (CH_2), 16.2 (CH_3), 15.3 (CH_3), 15.1 (CH_3). HR-MS (ESI$^+$, CH_2Cl_2/CH_3CN): m/z 1494.6358 (calcd m/z 1494.6329 for $C_{92}H_{82}N_8Pt^+$).

Monoprotonated Monometallic Pt^{II} Complex, H_3PtL^+. The monometallic complex **H_2PtL** was protonated with 1 equiv of TFA and was not isolated. The addition of 1,8-diazabicyclo[5.4.0]undec-7-ene (DBU) indicated reversibility of protonation/deprotonation. UV−vis [CH_2Cl_2/1% TFA; λ, nm (ε, M^{-1} cm^{-1})]: 786 (19000), 646 (44600), 565 (19300), 469 (23700), 396 (75600), 304 (34400), 257 (43400). For UV−vis titration spectra and low-temperature ^{1}H NMR titration spectra, see the Supporting Information.

Diprotonated Monometallic Pt^{II} Complex, H_4PtL^{2+}. The monometallic complex **H_2PtL** was protonated with 2 equiv of TFA in situ in order to obtain ^{1}H and ^{13}C NMR spectra; it was not isolated. The addition of DBU indicated reversibility of protonation/deprotonation. UV−vis [CH_2Cl_2/1% TFA; λ, nm (ε, M^{-1} cm^{-1})]: 773 (23200), 634 (47200), 457 (21000), 380 (81100), 304 (33600), 257 (43500). ^{1}H NMR (500 MHz, CD_2Cl_2/1% TFA, 298 K): δ 16.59 (br s, 2H, pz-NH), 12.83 (sharp s, 2H, pyrr-NH), 7.64 (d, J = 6.8 Hz, 2H, Ph), 7.52 (m, 3H, Ph), 7.45 (m, 2H, Ph), 7.41 (m, 3H, Ph), 7.12 (t, J = 8.4 Hz, 4H, Ph), 7.01 (m, 4H, Ph), 6.93 (m, 2H, Ph), 6.89 (dt, J = 7.3 Hz, 2H, Ph), 6.85 (m, 6H, Ph), 6.80 (m, 2H, Ph), 6.73 (m, 2H, Ph), 6.66 (m, 2H, Ph), 6.42 (d, J = 7.5 Hz, 2H, Ph), 6.31 (t, J = 7.5 Hz, 2H, Ph), 5.79 (d, J = 7.8 Hz, 2H, Ph), 2.10 (sextet, J = 7.3 Hz, 2H, CH_2), 2.00 (sextet, J = 7.4 Hz, 2H, CH_2), 1.85 (sextet, J = 7.6 Hz, 2H, CH_2), 1.75 (sextet, J = 7.3 Hz, 4H, CH_2), 1.66 (sextet, J = 7.4 Hz, 2H, CH_2), 1.39 (sextet, J = 7.4 Hz, 2H, CH_2), 1.28 (sextet, J = 7.3 Hz, 2H, CH_2), 0.69 (t, J = 7.4 Hz, 6H, CH_3), 0.62 (t, J = 7.5 Hz, 6H, CH_3), 0.59 (t, J = 7.5 Hz, 6H, CH_3), 0.55 (t, J = 7.5 Hz, 6H, CH_3). ^{13}C NMR (125 MHz, CD_2Cl_2/1% TFA, 298 K): δ 160.6 (C_q), 160.3 (C_q), 160.2 (C_q-pyrr), 154.2 (C_q-pyrr), 149.6 (C_q-pyrr), 147.8 (C_q-pyrr), 146.3 (C_q-pyrr), 145.3 (C_q), 145.1 (C_q-pyrr), 144.9 (C_q), 144.5 (C_q-pyrr), 142.2 (C_q), 138.7 (C_q), 138.0 (C_q), 137.1 (C_q), 135.4 (C_q), 134.8 (Ph), 134.3 (Ph), 134.1 (Ph), 132.31 (Ph), 132.26 (Ph), 132.13 (Ph), 132.08 (Ph), 132.03 (Ph), 130.5 (Ph), 129.1 (Ph), 128.9 (Ph), 128.7 (Ph), 128.6 (Ph), 128.4 (Ph), 128.1 (Ph), 127.9 (Ph), 127.3 (Ph), 127.2 (Ph), 127.1 (Ph), 127.0 (Ph), 126.8 (Ph), 125.9 (Ph), 122.9 (C_q), 121.3 (C_q), 118.4 (C_q), 116.1 (C_q), 111.4 (C_q), 106.1 (C_q), 20.0 (CH_2), 19.3 (CH_2), 19.1 (CH_2), 18.8 (CH_2), 16.2 (CH_3), 15.7 (CH_3), 14.52 (CH_3), 14.47 (CH_3). ^{195}Pt NMR (107 MHz, CD_2Cl_2/1% TFA, 298 K): δ −2203. For UV−vis and low-temperature ^{1}H NMR titration spectra, see the Supporting Information.

Heterobimetallic Ni^{II}/Pd^{II} Complex, NiPdL. To a solution of **H_2NiL** (23.6 mg, 17.4 μmol) in 10 mL of $C_2H_4Cl_2$-1,2 was added $Pd(OAc)_2$ (9.1 mg, 40.5 μmol, 2.3 equiv), and the solution was brought to reflux for 1 h. The solution changed from dark green-blue to purple. The solvent was removed under reduced pressure and the residue purified by column chromatography. After solvent removal again from the main fraction, the product was recrystallized from CH_2Cl_2 layered with MeOH at 0 °C to provide crystalline **NiPdL** (13.5 mg, 53% yield). Alternatively, beginning with a solution of **H_2PdL** (11.6 mg, 8.3 μmol) in $C_2H_4Cl_2$-1,2 (4 mL) was added $Ni(OAc)_2{\cdot}4H_2O$ (4.4 mg, 17.7 μmol) and EtOH (2 mL). The solution was refluxed, and the reaction was complete within 10 min. Purification via column chromatography and recrystallization from THF layered with MeOH at 0 °C gave crystalline **NiPdL** (8.9 mg, 73% yield). R_f = 0.84 (silica−2:1 hexane/EtOAc). ^{1}H NMR (500 MHz, CD_2Cl_2): δ 7.75 (d, J = 6.7 Hz, 2H, Ph), 7.65 (d, J = 7.0 Hz, 2H, Ph), 7.52−7.48 (m, 6H, Ph), 7.22 (d, J = 7.6 Hz, 2H, Ph), 7.02 (m, 4H, Ph), 6.95−6.90 (m, 10H, Ph), 6.74 (m, 4H, Ph), 6.66 (t, J = 7.4 Hz, 2H, Ph), 6.61 (t, J = 7.5 Hz, 2H, Ph), 6.49 (q, J = 8.1 Hz, 4H, Ph), 6.28 (d, J = 7.7 Hz, 2H, Ph), 2.06 (overlapping sextets, J = 7.0 Hz, 8H, CH_2), 1.77 (sextet, J = 7.5 Hz, 2H, CH_2), 1.64 (sextet, J = 7.3 Hz, 2H, CH_2), 1.40 (overlapping sextets, J = 7.3 Hz, 4H, CH_2), 0.69 (t, J = 7.5 Hz, 6H, CH_3), 0.62 (overlapping t, J = 7.3 Hz, 12H, CH_3), 0.53 (t, J = 7.4 Hz, 6H, CH_3). ^{13}C NMR (125 MHz, CD_2Cl_2): δ 157.9 (C_q), 156.7 (C_q), 156.2 (C_q), 152.5 (C_q), 149.1 (C_q), 147.3 (C_q), 146.7 (C_q), 146.4 (C_q), 145.6 (C_q), 145.4 (C_q), 139.1 (C_q), 138.7 (C_q), 137.1 (C_q), 136.0 (C_q), 134.0 (Ph), 133.5 (Ph), 133.4 (Ph), 133.3 (Ph), 133.2 (Ph), 132.0 (Ph), 131.9 (Ph), 131.6 (Ph), 131.4 (Ph), 128.0 (Ph), 127.9 (Ph), 127.7 (Ph), 127.7 (Ph), 127.2 (Ph), 127.1 (Ph), 126.6 (Ph), 126.5 (Ph), 126.4 (Ph), 126.3 (Ph), 124.9 (Ph), 123.9 (C_q), 118.8 (C_q), 109.9 (C_q), 108.7 (C_q), 19.3 (CH_2), 19.2 (CH_2), 18.9 (CH_2), 18.7 (CH_2), 15.8 (CH_3), 15.7 (CH_3), 15.3 (CH_3), 15.1 (CH_3). UV−vis [CH_2Cl_2; λ, nm (ε, M^{-1} cm^{-1})]: 718 (22400), 543 (30700), 512 (22100), 381 (62300), 323 (37800), 278 (46000). HR-MS (ESI$^+$, CH_2Cl_2/CH_3CN): m/z 1462.4887 (calcd m/z 1462.4905 for $C_{92}H_{80}N_8NiPd^+$).

Heterobimetallic Ni^{II}/Pt^{II} Complex, NiPtL. To a solution of **H_2NiL** (51.3 mg, 37.8 μmol) in 20 mL of $C_2H_4Cl_2$-1,2 (20 mL) was added PtI_2 (57.3 mg, 128 μmol), $NaOAc{\cdot}3H_2O$ (14.1 mg, 104 μmol), and 8 mL of MeCN. The reaction was brought to reflux for 21 h. Column chromatography and collection of the nonpolar pinkish-brown fraction, followed by recrystallization, afforded **NiPtL** (19.4 mg, 33% yield). Alternatively, starting with **H_2PtL** (16.3 mg, 10.9 μmol) dissolved in $C_2H_4Cl_2$-1,2 (6 mL), $Ni(OAc)_2{\cdot}4H_2O$ (7.3 mg, 29.3 μmol) and EtOH (2 mL) were added, and the resulting solution was heated to reflux for 10 min. Purification via column chromatography, evaporation to dryness, and recrystallization gave **NiPtL** (11.9 mg, 70%). R_f = 0.84 (silica−2:1 hexane/EtOAc). ^{1}H NMR (500 MHz, CD_2Cl_2, 298 K): δ 7.72 (d, J = 6.7 Hz, 2H, Ph), 7.60 (d, J = 6.3 Hz, 2H, Ph), 7.54−7.42 (m, 6H, Ph), 7.30 (d, J = 6.9 Hz, 2H, Ph), 6.99−6.86 (m, 12H, Ph), 6.77 (d, J = 6.8 Hz, 2H, Ph), 6.70−6.66 (m, 4H, Ph), 6.62 (d, J = 7.5 Hz, 2H, Ph), 6.51 (dt, J = 7.8 and 7.2 Hz, 4H, Ph), 6.37 (d, J = 7.2 Hz, 2H, Ph), 6.26 (d, J = 7.0 Hz, 2H, Ph), 2.07−1.99 (4 overlapping sextets, 8H, CH_2), 1.64 (sextet, J = 7.2 Hz, 2H, CH_2), 1.53 (sextet obscured by H_2O signal, J = 6.9 Hz, 2H, CH_2), 1.35 (2 overlapping sextets, J = 7.3 Hz, 4H, CH_2), 0.65 (t, J = 7.4 Hz, 6H, CH_3), 0.58 (t, J = 7.7 Hz, 6H, CH_3), 0.56 (t, J = 7.9 Hz, 6H, CH_3), 0.50 (t, J = 7.4 Hz, 6H, CH_3). ^{13}C NMR (125 MHz, CD_2Cl_2, 298 K): δ 158.8 (C_q), 153.9 (C_q), 152.7 (C_q), 151.7 (C_q), 149.5 (C_q), 147.1 (C_q), 146.2 (C_q), 145.6 (C_q), 144.6 (C_q), 139.3 (C_q), 139.1 (C_q), 136.9 (C_q), 136.7 (C_q), 134.7 (C_q), 134.1 (Ph), 133.9 (Ph), 133.8 (Ph), 133.3 (Ph), 133.0 (Ph), 132.7 (Ph), 132.5 (Ph), 131.4 (Ph), 128.5 (Ph), 128.4 (Ph), 128.1 (Ph), 128.0 (Ph), 127.7 (Ph), 127.6 (Ph), 127.5 (Ph), 127.4 (Ph), 127.1 (Ph), 126.9 (Ph), 126.84 (Ph), 126.83 (Ph), 125.3 (Ph), 123.3 (C_q), 119.4 (C_q), 109.1 (C_q), 108.9 (C_q), 19.9 (CH_2), 19.7 (CH_2), 19.4 (CH_2), 19.2 (CH_2), 16.5 (CH_3), 16.2 (CH_3), 15.7 (CH_3), 15.6 (CH_3). ^{195}Pt NMR (107 MHz, CD_2Cl_2, 298 K): δ −2519. UV−vis [CH_2Cl_2; λ, nm (ε, M^{-1} cm^{-1})]: 754 (16900), 532 (27100), 499 (22300), 418 (40800), 379 (53400), 326 (37500), 274 (45400). HR-MS (ESI$^+$, CH_2Cl_2/CH_3CN): m/z 1550.5511 (calcd m/z 1550.5513 for $C_{92}H_{80}N_8NiPt^+$).

Heterobimetallic Pd^{II}/Pt^{II} Complex, PdPtL. Monometalated **H_2PdL** (25.7 mg, 18.3 μmol) could be combined with PtI_2 (32.9 mg, 73.3 μmol) and $NaOAc{\cdot}3H_2O$ (7.2 mg, 52.9 μmol) in $C_2H_4Cl_2$-1,2

https://dx.doi.org/10.1021/acs.inorgchem.0c00714
Inorg. Chem. XXXX, XXX, XXX−XXX

(18 mL)/MeCN (6 mL). The contents were refluxed for 6 h. Purification was performed using column chromatography to collect the nonpolar pinkish-brown fraction. Recrystallization gave **PdPtL** (12.9 mg, 44%), and **H_2PdL** could be recovered (<15%). Alternatively, **H_2PtL** (12.5 mg, 8.36 μmol) was combined with $Pd(OAc)_2$ (3.9 mg, 17.4 μmol) in $C_2H_4Cl_2$-1,2 (8 mL) and refluxed for less than 10 min, and then the solvent was removed by rotary evaporation and purified via column chromatography to elute the nonpolar mauve/pinkish-brown fraction. Recrystallization from THF layered with MeOH provided **PdPtL** (10.2 mg, 76%). R_f = 0.85 (silica−2:1 hexane/EtOAc). ^{1}H NMR (500 MHz, CD_2Cl_2, 298 K): δ 7.77 (d, J = 6.7 Hz, 2H, Ph), 7.73 (d, J = 6.6 Hz, 2H, Ph), 7.52−7.48 (m, 6H, Ph), 7.12−7.09 (m, 2H, Ph), 7.04 (d, J = 7.6 Hz, 2H, Ph), 6.94−6.87 (m, 12H, Ph), 6.76−6.71 (m, 2H, Ph), 6.70−6.64 (m, 4H, Ph), 6.60 (t, J = 7.5 Hz, 2H, Ph), 6.48 (t, J = 7.6 Hz, 4H, Ph), 6.24 (d, J = 7.6 Hz, 2H, Ph), 2.09−1.91 (4 overlapping sextets, 8H, CH_2), 1.57 (2 overlapping sextets, 4H, CH_2), 1.37 (sextet, J = 7.4 Hz, 4H, CH_2), 0.58 (t, J = 7.3 Hz, 12H, CH_3), 0.47−0.44 (2 overlapping t, J = 7.5 Hz, 12H, CH_3. ^{13}C NMR (125 MHz, CD_2Cl_2, 298 K): δ 157.4 (C_q), 153.0 (C_q), 152.4 (C_q), 148.1 (C_q), 147.7 (C_q), 147.4 (C_q), 146.6 (C_q), 145.7 (C_q), 145.3 (C_q), 144.1 (C_q), 139.5 (C_q), 139.4 (C_q), 137.7 (C_q), 136.8 (C_q), 134.8 (Ph), 134.5 (Ph), 134.2 (Ph), 133.5 (Ph), 133.0 (Ph), 132.9 (Ph), 132.4 (Ph), 131.6 (Ph), 128.6 (Ph), 128.5 (Ph), 128.2 (Ph), 128.1 (Ph), 127.7 (Ph), 127.54 (Ph), 127.45 (Ph), 127.03 (Ph), 126.97 (Ph), 126.9 (Ph), 126.4 (Ph), 125.3 (Ph), 123.7 (C_q), 122.5 (C_q), 110.2 (C_q), 109.0 (C_q), 19.9 (CH_2), 19.6 (CH_2), 19.4 (CH_2), 19.3 (CH_2), 16.5 (CH_3), 16.1 (CH_3), 15.7 (CH_3), 15.6 (CH_3). ^{195}Pt NMR (107 MHz, CD_2Cl_2, 298 K): δ −2372. UV−vis [CH_2Cl_2; λ, nm (ε, M^{-1} cm^{-1})]: 738 (27400), 676 (16300), 620 (9500), 526 (37200), 500 (23900), 393 (55900), 321 (38300), 258 (54200). HR-MS (ESI$^+$, CH_2Cl_2/CH_3CN): m/z 1598.5205 (calcd m/z 1598.5213 for $C_{92}H_{80}N_8PdPt^+$).

■ ASSOCIATED CONTENT

Supporting Information

The Supporting Information is available free of charge at https://pubs.acs.org/doi/10.1021/acs.inorgchem.0c00714.

Synthetic procedures, analytical and spectroscopic data, and reproduction of the key spectra of all compounds studied, including their HR-MS, 1D and 2D ^{1}H, ^{13}C, and ^{195}Pt NMR spectra; experimental details for the MCD spectra and DFT/TDDFT calculations; experimental details for the crystal structure determinations of **Pt_2L**, **NiPdL**, **NiPtL**, and **PdPtL** (PDF)

Accession Codes

CCDC 1987503−1987506 contain the supplementary crystallographic data for this paper. These data can be obtained free of charge via www.ccdc.cam.ac.uk/data_request/cif, or by emailing data_request@ccdc.cam.ac.uk, or by contacting The Cambridge Crystallographic Data Centre, 12 Union Road, Cambridge CB2 1EZ, UK; fax: +44 1223 336033.

■ AUTHOR INFORMATION

Corresponding Authors

Victor N. Nemykin − *Department of Chemistry, University of Manitoba, Winnipeg, Manitoba R3T 2N2, Canada;* orcid.org/0000-0003-4345-0848; Email: victor.nemykin@umanitoba.ca

Christian Brückner − *Department of Chemistry, University of Connecticut, Storrs, Connecticut 06269-3060, United States;* orcid.org/0000-0002-1560-7345; Email: c.bruckner@uconn.edu

Franc Meyer − *Institute for Inorganic Chemistry, University of Göttingen, D-37077 Göttingen, Germany;* orcid.org/0000-0002-8613-7862; Email: franc.meyer@chemie.uni-goettingen.de

Authors

Sarina J. Dorazio − *Institute for Inorganic Chemistry, University of Göttingen, D-37077 Göttingen, Germany; Department of Chemistry, University of Connecticut, Storrs, Connecticut 06269-3060, United States*

Anastasia Vogel − *Institute for Inorganic Chemistry, University of Göttingen, D-37077 Göttingen, Germany*

Sebastian Dechert − *Institute for Inorganic Chemistry, University of Göttingen, D-37077 Göttingen, Germany;* orcid.org/0000-0002-2864-2449

Dustin E. Nevonen − *Department of Chemistry, University of Manitoba, Winnipeg, Manitoba R3T 2N2, Canada*

Complete contact information is available at: https://pubs.acs.org/10.1021/acs.inorgchem.0c00714

Author Contributions

The manuscript was written through contributions of all authors. S.J.D. and A.V. performed all syntheses, and S.J.D. performed all electrochemical investigations. S.D. performed the X-ray diffractometry studies. D.E.N. and V.N.N. recorded the MCD spectra and conducted all DFT and TDDFT calculations. C.B. and F.M. conceived the study. All authors have given approval to the final version of the manuscript.

Funding

This work was supported by the Alexander von Humboldt Stiftung (postdoctoral fellowship to S.J.D.), the Studienstiftung des deutschen Volkes (Ph.D. fellowship to A.V.), NSERC, CFI, WestGrid, and Minnesota Supercomputing Institute (all to V.N.N.), U.S. National Science Foundation under Grants CHE-1465133 and CHE-1800361 (to C.B.), and the University of Göttingen (to F.M.).

Notes

The authors declare no competing financial interest.

■ ACKNOWLEDGMENTS

We thank Jörg Teichgräber, Ralf Schöne, and Michael John (all of University of Göttingen) for technical assistance and Massimiliano Delferro (Argonne National Laboratory) for helpful discussions.

■ REFERENCES

(1) Sessler, J. L.; Weghorn, S. *Expanded, Contracted & Isomeric Porphyrins*; Pergamon Press: New York, 1997.

(2) Saito, S.; Osuka, A. Expanded porphyrins: Intriguing structures, electronic properties, and reactivities. *Angew. Chem., Int. Ed.* **2011**, *50* (19), 4342−4373.

(3) Roznyatovskiy, V. V.; Lee, C.-H.; Sessler, J. L. π-Extended isomeric and expanded porphyrins. *Chem. Soc. Rev.* **2013**, *42* (5), 1921−1933.

(4) Szyszko, B.; Latos-Grażyński, L. Core chemistry and skeletal rearrangements of porphyrinoids and metalloporphyrinoids. *Chem. Soc. Rev.* **2015**, *44* (11), 3588−3616.

(5) Tanaka, T.; Osuka, A. Chemistry of *meso*-aryl-substituted expanded porphyrins: Aromaticity and molecular twist. *Chem. Rev.* **2017**, *117* (4), 2584−2640.

(6) Szyszko, B.; Białek, M. J.; Pacholska-Dudziak, E.; Latos-Grażyński, L. Flexible porphyrinoids. *Chem. Rev.* **2017**, *117* (4), 2839−2909.

(7) Bauer, V. J.; Clive, D. L. J.; Dolphin, D.; Paine, J. B., III; Harris, F. L.; King, M. M.; Loder, J.; Wang, S. W. C.; Woodward, R. B.

Sapphyrins: Novel aromatic pentapyrrolic macrocycles. *J. Am. Chem. Soc.* **1983**, *105* (21), 6429−6436.

(8) Chatterjee, T.; Srinivasan, A.; Ravikanth, M.; Chandrashekar, T. K. Smaragdyrins and sapphyrins analogues. *Chem. Rev.* **2017**, *117* (4), 3329−3376.

(9) Neves, M. G. P. M. S.; Martins, R. M.; Tome, A. C.; Silvestre, A. J. D.; Silva, A. M. S.; Felix, V.; Cavaleiro, J. A. S.; Drew, M. G. B. *meso*-Substituted expanded porphyrins: New and stable hexaphyrins. *Chem. Commun.* **1999**, 385−386.

(10) Sessler, J. L.; Seidel, D.; Bucher, C.; Lynch, V. [26]Hexaphyrin-(1.1.1.1.0.0): An all-aza isomer of rubyrin with an inverted pyrrole subunit. *Chem. Commun.* **2000**, 1473−1474.

(11) Sessler, J. L.; Seidel, D.; Vivian, A. E.; Lynch, V.; Scott, B. L.; Keogh, D. W. Hexaphyrin(1.0.1.0.0.0): An expanded porphyrin ligand for the actinide cations uranyl (UO_2^{2+}) and neptunyl (NpO^{2+}). *Angew. Chem., Int. Ed.* **2001**, *40* (3), 591−594.

(12) Suzuki, M.; Osuka, A. Improved synthesis of *meso*-aryl-substituted [26]hexaphyrins. *Org. Lett.* **2003**, *5* (21), 3943−3946.

(13) Mori, S.; Shimizu, S.; Taniguchi, R.; Osuka, A. Group 10 metal complexes of *meso*-aryl-substituted [26]hexaphyrins with a metal-carbon bond. *Inorg. Chem.* **2005**, *44* (12), 4127−4129.

(14) Sessler, J. L.; Seidel, D.; Lynch, V. Synthesis of [28]-heptaphyrin(1.0.0.1.0.0.0) and [32]octaphyrin(1.0.0.0.1.0.0.0) via a directed oxidative ring closure: The first expanded porphyrins containing a quaterpyrrole subunit. *J. Am. Chem. Soc.* **1999**, *121* (48), 11257−11258.

(15) Geier, G. R., III; Grindrod, S. C. *meso*-Substituted [34]-octaphyrin(1.1.1.0.1.1.1.0) and corrole formation in reactions of a dipyrromethanedicarbinol with 2,2'-bipyrrole. *J. Org. Chem.* **2004**, *69* (19), 6404−6412.

(16) Kido, H.; Shin, J.-Y.; Shinokubo, H. Selective synthesis of a [32]octaphyrin(1.0.1.0.1.0.1.0) bis(palladium) complex by a metal-templated strategy. *Angew. Chem., Int. Ed.* **2013**, *52* (51), 13727−13730.

(17) Misra, R.; Chandrashekar, T. K. Structural diversity in expanded porphyrins. *Acc. Chem. Res.* **2008**, *41* (2), 265−279.

(18) Stępień, M.; Szyszko, B.; Latos-Grażyński, L. Three-level topology switching in a molecular Möbius band. *J. Am. Chem. Soc.* **2010**, *132* (9), 3140−3152.

(19) Frensch, L. K.; Proepper, K.; John, M.; Demeshko, S.; Brückner, C.; Meyer, F. Siamese-twin porphyrin: A pyrazole-based expanded porphyrin providing a bimetallic cavity. *Angew. Chem., Int. Ed.* **2011**, *50* (6), 1420−1424.

(20) Ho, I. T.; Zhang, Z.; Ishida, M.; Lynch, V. M.; Cha, W.-Y.; Sung, Y. M.; Kim, D.; Sessler, J. L. A hybrid macrocycle with a pyridine subunit displays aromatic character upon uranyl cation complexation. *J. Am. Chem. Soc.* **2014**, *136* (11), 4281−4286.

(21) Oh, J.; Mori, H.; Sung, Y. M.; Kim, W.; Osuka, A.; Kim, D. Switchable π-electronic network of bis(α-oligothienyl)-substituted hexaphyrins between helical versus rectangular circuit. *Chem. Sci.* **2016**, *7* (3), 2239−2245.

(22) Abebayehu, A.; Dutta, R.; Lee, C.-H. Synthesis, characterization and properties of expanded pyriporphyrins: A new family of alkylidenyl porphyrin homologues bearing *meso*-exocyclic double bonds. *Chem. - Eur. J.* **2016**, *22* (39), 13850−13856.

(23) Cha, W.-Y.; Kim, T.; Ghosh, A.; Zhang, Z.; Ke, X.-S.; Ali, R.; Lynch, V. M.; Jung, J.; Kim, W.; Lee, S.; Fukuzumi, S.; Park, J. S.; Sessler, J. L.; Chandrashekar, T. K.; Kim, D. Bicyclic Baird-type aromaticity. *Nat. Chem.* **2017**, *9*, 1243.

(24) Setsune, J.-i.; Toda, M.; Yoshida, T.; Imamura, K.; Watanabe, K. The synthesis and dynamic structures of multinuclear complexes of large porphyrinoids expanded by phenylene and thienylene spacers. *Chem. - Eur. J.* **2015**, *21* (36), 12715−12727.

(25) Chatterjee, T.; Theophall, G. G.; Silva, K. I.; Lakshmi, K. V.; Ravikanth, M. Synthesis and quantum mechanical studies of a highly stable ferrocene-incorporated expanded porphyrin. *Inorg. Chem.* **2016**, *55* (14), 6873−6881.

(26) Sessler, J. L.; Vivian, A. E.; Seidel, D.; Burrell, A. K.; Hoehner, M.; Mody, T. D.; Gebauer, A.; Weghorn, S. J.; Lynch, V. Actinide expanded porphyrin complexes. *Coord. Chem. Rev.* **2001**, *216−217*, 411−434.

(27) Brewster, J. T.; Mangel, D. N.; Gaunt, A. J.; Saunders, D. P.; Zafar, H.; Lynch, V. M.; Boreen, M. A.; Garner, M. E.; Goodwin, C. A. P.; Settineri, N. S.; Arnold, J.; Sessler, J. L. In-plane thorium(IV), uranium(IV), and neptunium(IV) expanded porphyrin complexes. *J. Am. Chem. Soc.* **2019**, *141* (44), 17867−17874.

(28) Gisselbrecht, J. P.; Gross, M.; Vogel, E.; Scholz, P.; Bröring, M.; Sessler, J. L. Redox properties of hemiporphycene and isoporphycene. Comparison with those of porphyrin and other porphyrin isomers, porphycene and corrphycene. *J. Electroanal. Chem.* **2001**, *507* (1−2), 244−249.

(29) Bley-Escrich, J.; Gisselbrecht, J.-P.; Michels, M.; Zander, L.; Vogel, E.; Gross, M. Electrochemical and spectroelectrochemical investigations of mono- and binuclear cobalt(II) complexes of "figure-eight" octapyrrolic macrocycles. *Eur. J. Inorg. Chem.* **2004**, *3*, 492−499.

(30) Tanaka, Y.; Saito, S.; Mori, S.; Aratani, N.; Shinokubo, H.; Shibata, N.; Higuchi, Y.; Yoon, Z. S.; Kim, K. S.; Noh, S. B.; Park, J. K.; Kim, D.; Osuka, A. Metalation of expanded porphyrins: A chemical trigger used to produce molecular twisting and Möbius aromaticity. *Angew. Chem., Int. Ed.* **2008**, *47* (4), 681−684.

(31) Anguera, G.; Cha, W.-Y.; Moore, M. D.; Lee, J.; Guo, S.; Lynch, V. M.; Kim, D.; Sessler, J. L. Hexadecaphyrin-(1.0.0.0.1.1.0.1.1.0.0.0.1.1.0.1) : A dual site ligand that supports thermal conformational changes. *J. Am. Chem. Soc.* **2018**, *140* (11), 4028−4034.

(32) Blusch, L. K.; Hemberger, Y.; Pröpper, K.; Dittrich, B.; Witterauf, F.; John, M.; Bringmann, G.; Brückner, C.; Meyer, F. Siamese-twin porphyrin: A pyrazole-based expanded porphyrin of persistent helical conformation. *Chem. - Eur. J.* **2013**, *19* (19), 5868−5880.

(33) Mitevski, O.; Dechert, S.; Brückner, C.; Meyer, F. Siamese-twin porphyrins: Variation of two *meso*-aryl groups. *Eur. J. Inorg. Chem.* **2016**, 4814−4819.

(34) Vogel, A.; Dechert, S.; Brückner, C.; Meyer, F. Reaching across the divide: How monometalation of one binding pocket affects the empty binding pocket in a Siamese-twin porphyrin palladium complex. *Inorg. Chem.* **2017**, *56* (4), 2221−2232.

(35) Ahn, T. K.; Kwon, J. H.; Kim, D. Y.; Cho, D. W.; Jeong, D. H.; Kim, S. K.; Suzuki, M.; Shimizu, S.; Osuka, A.; Kim, D. Comparative photophysics of [26]- and [28]hexaphyrins(1.1.1.1.1.1): Large two-photon absorption cross section of aromatic [26]-hexaphyrins(1.1.1.1.1.1). *J. Am. Chem. Soc.* **2005**, *127* (37), 12856−12861.

(36) Yoon, Z. S.; Osuka, A.; Kim, D. Möbius aromaticity and antiaromaticity in expanded porphyrins. *Nat. Chem.* **2009**, *1* (2), 113−122.

(37) Latos-Grażyński. Bimetallic figure-eight octaphyrins split into four-pyrrolic macrocycles. *Angew. Chem., Int. Ed.* **2004**, *43* (39), 5124−5128.

(38) Tanaka, Y.; Hoshino, W.; Shimizu, S.; Youfu, K.; Aratani, N.; Maruyama, N.; Fujita, S.; Osuka, A. Thermal splitting of bis-Cu(II) octaphyrin(1.1.1.1.1.1.1.1) into two Cu(II) porphyrins. *J. Am. Chem. Soc.* **2004**, *126* (10), 3046−3047.

(39) Shimizu, S.; Tanaka, Y.; Youfu, K.; Osuka, A. Dicopper and disilver complexes of octaphyrin(1.1.1.1.1.1.1.1): Reversible hydrolytic cleavage of the pyrrolic ring to a keto-imine. *Angew. Chem., Int. Ed.* **2005**, *44* (24), 3726−3729.

(40) Vogel, A.; Dechert, S.; John, M.; Brückner, C.; Meyer, F. Siamese-twin porphyrin origami: Oxidative fusing and folding. *Chem. - Eur. J.* **2016**, *22* (7), 2307−2316.

(41) Blusch, L. K.; Craigo, K. E.; Martin-Diaconescu, V.; McQuarters, A. B.; Bill, E.; Dechert, S.; DeBeer, S.; Lehnert, N.; Meyer, F. Hidden non-innocence in an expanded porphyrin: Electronic structure of the Siamese-twin porphyrin's dicopper complex in different oxidation states. *J. Am. Chem. Soc.* **2013**, *135* (37), 13892−13899.

https://dx.doi.org/10.1021/acs.inorgchem.0c00714
Inorg. Chem. XXXX, XXX, XXX−XXX

(42) Blusch, L. K.; Mitevski, O.; Martin-Diaconescu, V.; Propper, K.; DeBeer, S.; Dechert, S.; Meyer, F. Selective synthesis and redox sequence of a heterobimetallic nickel/copper complex of the noninnocent Siamese-twin porphyrin. *Inorg. Chem.* **2014**, *53* (15), 7876−7885.

(43) Lee, W. W. S.; Wong, K. Y.; Li, X. M.; Leung, Y. B.; Chan, C. S.; Chan, K. S. Halogenated platinum porphyrins as sensing materials for luminescence-based oxygen sensors. *J. Mater. Chem.* **1993**, *3* (10), 1031−1035.

(44) Papkovsky, D. B.; Ponomarev, G. V.; Wolfbeis, O. S. Longwave luminescent porphyrin probes. *Spectrochim. Acta, Part A* **1996**, *52A* (12), 1629−1638.

(45) Grenoble, S.; Gouterman, M.; Khalil, G.; Callis, J.; Dalton, L. Pressure-sensitive paint (PSP): Concentration quenching of platinum and magnesium porphyrin dyes in polymeric films. *J. Lumin.* **2005**, *113* (1−2), 33−44.

(46) Amao, Y.; Okura, I. Optical oxygen sensor devices using metalloporphyrins. *J. Porphyrins Phthalocyanines* **2009**, *13* (11), 1111−1122.

(47) Spencer, J. A.; Ferraro, F.; Roussakis, E.; Klein, A.; Wu, J.; Runnels, J. M.; Zaher, W.; Mortensen, L. J.; Alt, C.; Turcotte, R.; Yusuf, R.; Cote, D.; Vinogradov, S. A.; Scadden, D. T.; Lin, C. P. Direct measurement of local oxygen concentration in the bone marrow of live animals. *Nature* **2014**, *508* (7495), 269−273.

(48) Pandey, G.; Chaudhari, R.; Joshi, B.; Choudhary, S.; Kaur, J.; Joshi, A. Fluorescent biocompatible platinum-porphyrin−doped polymeric hybrid particles for oxygen and glucose biosensing. *Sci. Rep.* **2019**, *9* (1), 5029−5039.

(49) Mercer-Smith, J. A.; Whitten, D. G. Photosensitization of stilbene isomerization by palladium and platinum porphyrins, an intermolecular quantum chain process. *J. Am. Chem. Soc.* **1978**, *100* (9), 2620−2625.

(50) Vakrat-Haglili, Y.; Weiner, L.; Brumfeld, V.; Brandis, A.; Salomon, Y.; McLlroy, B.; Wilson, B. C.; Pawlak, A.; Rozanowska, M.; Sarna, T.; Scherz, A. The microenvironment effect on the generation of reactive oxygen species by Pd-bacteriopheophorbide. *J. Am. Chem. Soc.* **2005**, *127* (17), 6487−6497.

(51) Huang, Y.-Y.; Balasubramanian, T.; Yang, E.; Luo, D.; Diers, J. R.; Bocian, D. F.; Lindsey, J. S.; Holten, D.; Hamblin, M. R. Stable synthetic bacteriochlorins for photodynamic therapy: Role of dicyano peripheral groups, central metal substitution (2H, Zn, Pd), and Cremophor EL delivery. *ChemMedChem* **2012**, *7* (12), 2155−2167.

(52) To, W.-P.; Liu, Y.; Lau, T.-C.; Che, C.-M. A robust palladium(II)−porphyrin complex as catalyst for visible light induced oxidative C-H functionalization. *Chem. - Eur. J.* **2013**, *19* (18), 5654−5664.

(53) Lau, K. S. F.; Zhao, S.; Ryppa, C.; Jockusch, S.; Turro, N. J.; Zeller, M.; Gouterman, M.; Khalil, G. E.; Brückner, C. Synthesis, structure, and optical properties of the platinum(II) complexes of indaphyrin and thiaindaphyrin. *Inorg. Chem.* **2009**, *48* (9), 4067−4074.

(54) Sommer, J. R.; Shelton, A. H.; Parthasarathy, A.; Ghiviriga, I.; Reynolds, J. R.; Schanze, K. S. Photophysical properties of near-infrared phosphorescent π-extended platinum porphyrins. *Chem. Mater.* **2011**, *23* (24), 5296−5304.

(55) Akhigbe, J.; Luciano, M.; Atoyebi, A. O.; Jockusch, S.; Brückner, C. Quinoline-annulated porphyrin platinum complexes as NIR emitters. *J. Porphyrins Phthalocyanines* **2020**, *24* (1−3), 386−393.

(56) Shannon, R. D. Revised effective ionic radii and systematic studies of interatomic distances in halides and chalcogenides. *Acta Crystallogr., Sect. A: Cryst. Phys., Diffr., Theor. Gen. Crystallogr.* **1976**, *A32* (5), 751−767.

(57) Yang, L.; Powell, D. R.; Houser, R. P. Structural variation in copper(I) complexes with pyridylmethylamide ligands: Structural analysis with a new four-coordinate geometry index, τ_4. *Dalton Trans.* **2007**, *9*, 955−964.

(58) Jentzen, W.; Simpson, M. C.; Hobbs, J. D.; Song, X.; Ema, T.; Nelson, N. Y.; Medforth, C. J.; Smith, K. M.; Veyrat, M.; Mazzanti, M.; Ramasseul, R.; Marchon, J. C.; Takeuchi, T.; Goddard, W. A.; Shelnutt, J. A. Ruffling in a series of nickel(II) *meso*-tetrasubstituted porphyrins as a model for the conserved ruffling of the heme of cytochromes c. *J. Am. Chem. Soc.* **1995**, *117* (45), 11085−11097.

(59) Jentzen, W.; Turowska-Tyrk, I.; Scheidt, W. R.; Shelnutt, J. A. Planar solid-state and solution structure of (porphyrinato)nickel(II) as determined by X-ray diffraction and resonance Raman spectroscopy. *Inorg. Chem.* **1996**, *35*, 3559−3567.

(60) Brückner, C.; Hyland, M. A.; Sternberg, E. D.; MacAlpine, J.; Rettig, S. J.; Patrick, B. O.; Dolphin, D. Preparation of [*meso*-tetraphenylchlorophinato]nickel(II) by stepwise deformylation of [*meso*-tetraphenyl-2,3-diformylsecochlorinato]nickel(II): Conformational consequences of breaking the structural integrity of nickel porphyrins. *Inorg. Chim. Acta* **2005**, *358* (10), 2943−2953.

(61) Priqueler, J. R. L.; Butler, I. S.; Rochon, F. D. An overview of ^{195}Pt nuclear magnetic resonance spectroscopy. *Appl. Spectrosc. Rev.* **2006**, *41* (3), 185−226.

(62) Milgrom, L. R.; Zuurbier, R. J.; Gascoyne, J. M.; Thompsett, D.; Moore, B. C. Platinum porphyrins. IV. Platinum-195 NMR spectra of some platinum complexes of *meso*- and β-substituted porphyrins. *Polyhedron* **1992**, *11* (14), 1779−1781.

(63) Lim, J. M.; Yoon, Z. S.; Shin, J.-Y.; Kim, K. S.; Yoon, M.-C.; Kim, D. The photophysical properties of expanded porphyrins: Relationships between aromaticity, molecular geometry and nonlinear optical properties. *Chem. Commun.* **2008**, *3*, 261−273.

(64) Arumugam, K.; Shaw, M. C.; Chandrasekaran, P.; Villagrán, D.; Gray, T. G.; Mague, J. T.; Donahue, J. P. Synthesis, structures, and properties of 1,2,4,5-benzenetetrathiolate linked group 10 metal complexes. *Inorg. Chem.* **2009**, *48* (22), 10591−10607.

(65) Mack, J.; Stillman, M. J., Electronic structures of metal phthalocyanine and porphyrin complexes from analysis of the UV-visible absorption and magnetic circular dichroism spectra and molecular orbital calculations. In *The Porphyrin Handbook*; Kadish, K. M., Smith, K. M., Guilard, R., Eds.; Academic Press: San Diego, CA, 2003; Vol. *16*, pp 43−116.

(66) Stillman, M.; Mack, J.; Kobayashi, N. Theoretical aspects of the spectroscopy of porphyrins and phthalocyanines. *J. Porphyrins Phthalocyanines* **2002**, *6* (4), 296−300.

(67) Rhoda, H. M.; Crandall, L. A.; Geier, G. R.; Ziegler, C. J.; Nemykin, V. N. Combined MCD/DFT/TDDFT study of the electronic structure of axially pyridine coordinated metallocorroles. *Inorg. Chem.* **2015**, *54* (10), 4652−4662.

(68) Rhoda, H. M.; Akhigbe, J.; Ogikubo, J.; Sabin, J. R.; Ziegler, C. J.; Brückner, C.; Nemykin, V. N. Magnetic circular dichroism spectroscopy of *meso*-tetraphenylporphyrin-derived hydroporphyrins and pyrrole-modified porphyrins. *J. Phys. Chem. A* **2016**, *120* (29), 5805−5815.

(69) Mack, J. Expanded, contracted, and isomeric porphyrins: Theoretical aspects. *Chem. Rev.* **2017**, *117* (4), 3444−3478.

(70) Kobayashi, N.; Inagaki, S.; Nemykin, V. N.; Nonomura, T. A novel hemiporphyrazine comprising three isoindolediimine and three thiadiazole units. *Angew. Chem., Int. Ed.* **2001**, *40* (14), 2710−2712.

(71) Nemykin, V. N.; Hadt, R. G.; Belosludov, R. V.; Mizuseki, H.; Kawazoe, Y. Influence of molecular geometry, exchange-correlation functional, and solvent effects in the modeling of vertical excitation energies in phthalocyanines using time-dependent density functional theory (TDDFT) and polarized continuum model TDDFT methods: Can modern computational chemistry methods explain experimental controversies? *J. Phys. Chem. A* **2007**, *111* (50), 12901−12913.

(72) Belosludov, R. V.; Nevonen, D.; Rhoda, H. M.; Sabin, J. R.; Nemykin, V. N. Simultaneous prediction of the energies of Q_x and Q_y bands and intramolecular charge-transfer transitions in benzoannulated and non-peripherally substituted metal-free phthalocyanines and their analogues: No standard TDDFT silver bullet yet. *J. Phys. Chem. A* **2019**, *123* (1), 132−152.

(73) Martynov, A. G.; Mack, J.; May, A. K.; Nyokong, T.; Gorbunova, Y. G.; Tsivadze, A. Y. Methodological survey of simplified TD-DFT methods for fast and accurate interpretation of UV−vis−NIR spectra of phthalocyanines. *ACS Omega* **2019**, *4* (4), 7265−7284.

https://dx.doi.org/10.1021/acs.inorgchem.0c00714
Inorg. Chem. XXXX, XXX, XXX−XXX

(74) Galinato, M. G. I.; Spolitak, T.; Ballou, D. P.; Lehnert, N. Elucidating the role of the proximal cysteine hydrogen-bonding network in ferric cytochrome P450cam and corresponding mutants using magnetic circular dichroism spectroscopy. *Biochemistry* **2011**, *50* (6), 1053−1069.

(75) Frisch, M. J.; Trucks, G. W.; Schlegel, H. B.; Scuseria, G. E.; Robb, M. A.; Cheeseman, J. R.; Scalmani, G.; Barone, V.; Mennucci, B.; Petersson, G. A.; Nakatsuji, H.; Caricato, M.; Li, X.; Hratchian, H. P.; Izmaylov, A. F.; Bloino, J.; Zheng, G.; Sonnenberg, J. L.; Hada, M.; Ehara, M.; Toyota, K.; Fukuda, R.; Hasegawa, J.; Ishida, M.; Nakajima, T.; Honda, Y.; Kitao, O.; Nakai, H.; Vreven, T.; Montgomery, J. A., Jr.; Peralta, J. E.; Ogliaro, F.; Bearpark, M. J.; Heyd, J.; Brothers, E. N.; Kudin, K. N.; Staroverov, V. N.; Kobayashi, R.; Normand, J.; Raghavachari, K.; Rendell, A. P.; Burant, J. C.; Iyengar, S. S.; Tomasi, J.; Cossi, M.; Rega, N.; Millam, N. J.; Klene, M.; Knox, J. E.; Cross, J. B.; Bakken, V.; Adamo, C.; Jaramillo, J.; Gomperts, R.; Stratmann, R. E.; Yazyev, O.; Austin, A. J.; Cammi, R.; Pomelli, C.; Ochterski, J. W.; Martin, R. L.; Morokuma, K.; Zakrzewski, V. G.; Voth, G. A.; Salvador, P.; Dannenberg, J. J.; Dapprich, S.; Daniels, A. D.; Farkas, Ö.; Foresman, J. B.; Ortiz, J. V.; Cioslowski, J.; Fox, D. J. *Gaussian 09*; Gaussian, Inc.: Wallingford, CT, 2009.

(76) Becke, A. D. Density-functional thermochemistry. III. The role of exact exchange. *J. Chem. Phys.* **1993**, *98* (7), 5648−5652.

(77) Godbout, N.; Salahub, D. R.; Andzelm, J.; Wimmer, E. Optimization of Gaussian-type basis sets for local spin density functional calculations. Part I. Boron through neon, optimization technique and validation. *Can. J. Chem.* **1992**, *70* (2), 560−571.

https://dx.doi.org/10.1021/acs.inorgchem.0c00714
Inorg. Chem. XXXX, XXX, XXX−XXX